SKYLAB PROGRAM

MSC-05538

EARTH RESOURCES EXPERIMENT PACKAGE

EREP GEOTHERMAL
FINAL REPORT

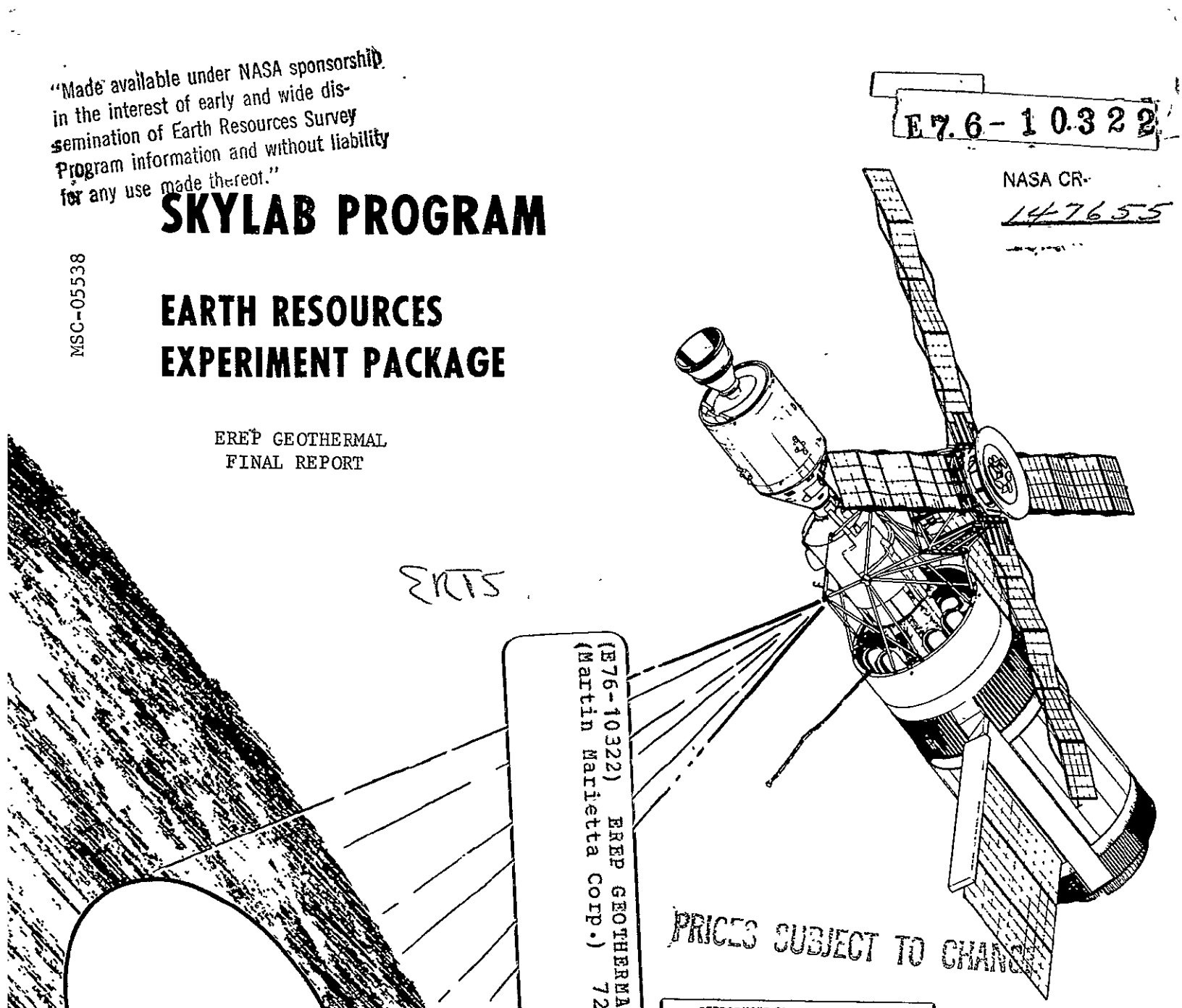

REISSUE
AUGUST 9, 1974

CONTRACT NAS8-24000
AMENDMENT MSC-14S

MARTIN MARIETTA
DENVER DIVISION

MSC-05538

SKYLAB PROGRAM

Earth Resources Experiment Package

EREP Geothermal

Final Report

August 1, 1974

Contract NAS8-24000
Amendment JSC-14S

Prepared by:

E. W. Johnston

A. L. Dunklee

D. C. Wychgram

Approved by:

L. P. Oldham
SPE Optical Sensors Lead

W. O. Nobles
EREP Program Manager

FOREWORD

This document is prepared by Martin Marietta Corporation and is submitted in accordance with the requirements of Annex I to Exhibit A, Statement of Work, Part I, Data Requirements List (DRL), dated May 21, 1970, of Contract NAS8-24000, Amendment JSC-14S, Line Item No. 320.

The effort for this task was performed under WBS No. 2216.

CONTENTS

CONTENTS
(Continued)

CONTENTS
(Continued)

CONTENTS
(Concluded)

1. INTRODUCTION

1.1 Purpose - The purpose of this document is to present the results of a study performed to evaluate the capability the SKYLAB S192 Multispectral Scanner thermal band for identifying Geothermal Sources.

1.2 Scope - This report uses the ground truth data and S192 thermal band data gathered during a nighttime pass and a daytime pass over The Geysers geothermal area in northern California. Digital processing was used to produce and improve thermal images from the S192 data.

1.3 Summary - A description of the ground site is presented along with the equipment and procedures used to obtain the ground truth data. The digital processing used to produce images from the S192 scanner data tapes are presented along with special algorithms for producing isothermal contour images. A resolution of image problems presented by the noisy detector array is described.

A reasonably good agreement was found for the radiometric temperatures calculated from the ground truth data and the radiometric temperatures measured by the S192 scanner. This investigation showed that the S192 scanner data could be used to create good thermal images, particularly with the X-5 detector array.

Because of the dominating effects of solar heating on the daytime thermal image, the nighttime thermal image is potentially more useful. With the limited amount of data available for this study it was not possible to decide conclusively whether or not the geothermal anomalies of The Geysers area would have been detectable without the associated development features. A full examination of the usefulness of S192 thermal data to geothermal exploration would require nighttime and daytime thermal images over a known but undeveloped geothermal area.

2. APPLICABLE DOCUMENTS

None Applicable.

3. ACQUISITION OF DATA

3.1 Geography and Topography of Site - The Geysers geothermal area is located in northern California, 110 km north-northwest of San Francisco in Sonoma County.

The topography of The Geysers area is dominated by northwest trending ridges and valleys with the primary geothermal activity occurring in the valley occupied by Big Sulphur Creek (see Topographic Map, Figure 3.7-4). Relief is on the order of 500 meters with the higher points in the area at about 1000 meters elevation. The climate is Mediterranean and vegetation consists of grass and assorted trees and brush.

3.2 Geothermal Development and History of Site - The geothermal significance of the area has been known for over a century; a health resort was constructed near naturally occurring hot springs around 1852. Although the first steam well was drilled in 1922, electrical power production did not commence until 1960. The Pacific Gas and Electric Co. installed an initial 12.5 kilowatt generator powered by steam from four wells. Since then, additional generators have been installed with present capacity being over 180,000 kilowatts. More power production capability is planned for the future.

There are many surface features associated with the geothermal anomaly at The Geysers area. Hot springs, with effluents ranging in temperature from 80° to 90°C, and steaming hydrothermally altered zones are present in the area. Uncapped steam wells are located in the area that allow steam to escape into the atmosphere that can be seen from several miles away. Large sets of cooling towers, associated with the generator plants, pass enough steam into the air so as to be visible on Skylab-EREP photography. These developments are shown in Figure 3.2-1.

3.3 Geology of Site - The geology of The Geysers area has a direct relationship to the occurrence and distribution of geothermal features. The area is underlain by the geologically complex Franciscan Formation (Mesozoic) which, in the immediate vicinity of The Geysers, consists of massive graywacke, shale, greenstone, chert beds and serpentized peridotite (see Moxham, 1969). Extrusive volcanic rocks exist near the report area. Cobb Mountain, located just northeast of the area is capped by rhyolite of Pliocene (Bailey, 1946) of Pleistocene (McNitt, 1968) age. The Clear Lake volcanic field (Pleistocene) extends to within 5 miles of The Geysers area.

The topographic, lithologic, and structural grain of the area is northwest trending. The Geysers area is situated on a downthrown structural block bounded by steeply dipping arcuate faults. McNitt's (1968) interpretation indicates the possibility of 15,000 feet of total vertical displacement. A linear zone of geothermal activity, which includes The Geysers area, extends for 21 miles along the northeast side of the downthrown block. It is probable that the large vertical displacement has brought up near the surface high temperature rocks to the northeast of the geothermal zone or that the faults have created a pathway for superheated fluids at depth to reach the surface. Garrison (1972) suggests that a shallow intrusive magma body, emplaced in Quaternary to Holocene time, is the source of heat. The fluid in the steam reservoir system is primarily from meteoric water although it is probable that some portion is derived from magma.

The hot springs of the area range in temperature between 60°C and 102°C. Steaming ground and associated gas vents have temperatures in the 90°C range. The electrical power production potential of proven steam reserves in the geothermal area amounts to about 200 megawatts (Moxham, 1969).

3.4 S192 Multispectral Scanner - The S192 multispectral scanner was an optical-mechanical scanner, together with a spectral dispersion system. The scanner assembly utilized a rotating mirror to perform a conical scanning of the scene viewed with a cone angle of 5.5 degrees about instrument axis (nadir) or 84.5 degrees elevation angle. The spectrally dispersed electromagnetic energy received from the earth's surface simultaneously irradiated 13 detectors. Each detector responded to a particular spectral region, and all 13 detectors covered spectral regions between 0.410 and 12.5 m. The spectral band coverage is given in Table 3.4-1. The curved scan pattern covered a swath of the earth's surface that was approximately 72.4 km (39.1 nmi) wide and selected lengths along the ground-track of Skylab. The content of each scanning arc was 1240 or 2480 pixels, depending upon the band (see Table 3.4-1). The instantaneous field of view (IFOV) is 79.25 meters (260 feet). A total of 94.792 scans occurred each second.

Each of the 13 detectors produced an electronic output signal that corresponded to the average value of the radiance currently being received in its particular spectral band from the spot on the earth's surface contained in the 0.182 milliradian instantaneous field of view. The electromagnetic energy was passed on for spectral analysis only during the front 116 (approximate) degrees of the 360 degree scanning cycle. During a part of the unused scanning cycle, the detectors viewed suitable calibration sources. Hence, radiometric calibration data was available between each pair of image scan lines. The calibration sources for band 13 were two blackbody references at 320°K and 260°K, and for bands 1 through 12 a tungsten lamp was used.

For the purposes of this study, a primitive S192 PDP to CYBER interface tape was obtained for the two EREP passes.* (The tape format is specified in TR543). (See reference 4). These data were not geometrically corrected or modified by TR524 processing. Some of the processing presented in this present report requires that the data not be modified by TR524. The low data sampling rate of 1240 pixels/scan was employed and found to be sufficient for the processing required.

3.5 Ground Instrumentation - The following describes the ground instrumentation used for both Skylab-EREP passes.

The Barnes PRT-5 Radiation Thermometer senses thermal emittance in the 8 to 14 μm region. It has a sensitivity range of -20° to 75°C, a field of view of 2°, an accuracy of 0.5°C, and a stability of better than 1%. Two methods of calibration were used to calibrate the PRT-5. For temperatures below ambient temperature a blackbody temperature equivalent was immersed in a dry ice and acetone controlled bath and allowed to stabilize for one-half hour at each temperature measured. The temperature of the bath was monitored by a stem thermometer traceable to the National Bureau of Standards. For ambient and higher temperatures, a blackbody standard, traceable to N.B.S., was allowed to stabilize at given temperatures.

The PRT-5 was used from a helicopter in order to make rapid and thorough measurements. The PRT-5 sensor head was

* The following are the exact GMT's used for Geyser's data. For pass 91, (January) the interval is 19 hr. 41 min. 8.96 to 11.66 sec. For pass 68, (December) the interval is 11 hr. 36 min. 6.25 to 8.93 sec.

pointed as directly down as possible out of the helicopter window. The reference blackbody cavity control was continuously monitored in order to assure that no adverse effects on the data occurred.

The 2^{o} field of view covers a 21.3 meter diameter spot on the ground from 2000 feet (625 meters) altitude. Since the sensor head was handheld, it can be expected that a combination of aircraft roll and operator pointing errors could amount to about 10^{o} off vertical (nadir) location error (105 meters) from the estimated ground track. This potential displacement of data points, in conjunction with possible errors in plotting the actual flightline ground tracks (especially for the night-time mission), is considered in the comparison of ground truth data and S192 data later in this report.

The near surface meteorology measurements were made with a sling psychrometer, dry and wet bulb temperatures - accuracy of $\pm$ 1^{o}F; a handheld cup anemometer - accuracy of $\pm$ 2 m.p.h., and an aneroid barometer - accuracy of $\pm$ .1 in. of Hg.

The atmospheric temperature and humidity vertical profiles were obtained by releasing a Colspan Environmental Systems Co. (Boulder, Colorado) radiosonde from a helicopter. Data from a coated bead thermistor (temperature) and a carbon element hygristor (ML-476) were telemetered to a ground receiving station (403 MHz). The radiosonde descended to the surface on a parachute at approximately 25 - 26 ft/sec. These data were recorded on two identical stripcharts during the radiosonde descent. To calibrate the radiosonde temperature sensor/recorder, an internal potentiometer (within the ground station) was set just prior to being loaded into the helicopter. This potentiometer adjusted the slope of the current vs. temperature response, which was set according to the measured (mercury thermometer) ambient air temperature. Because the current output of the sensor was linear with respect to temperature, the atmospheric profile temperatures could then be accurately determined based on the ground-based mercury thermometer calibration. To calibrate the humidity sensor, just prior to being loaded in the helicopter, the hygristor was replaced with a precise 20k ohm resistor. This value of resistance corresponded to a humidity of 33%, an internal potentiometer was then set to correspond to this humidity. Calibration tables relating the outputs of the bead thermistor and hygristor sensors to temperature and humidity were subsequently used to derive the absolute atmospheric

temperatures and humidities. These data were then used to calculate the values for vapor concentration.

A problem encountered on both missions (December 73 and January 73) was loss of signal from the radiosonde due to line-of-sight problems with the surrounding mountain ridges. The location of the ground station was based on an acceptable helicopter landing site and a desire to be near the valley floor elevation. This, in turn, required the dropsonde to descend into the same valley as the ground station. Unpredicted winds carried it into the adjacent valley with the intervening ridge cutting off signal at elevations of approximately 6300 ft. A.S.L. for the December mission and at 5200 ft. A.S.L. for the January mission.

3.6 December Night Mission Ground Truth Data - The first mission was on December 18, 1973 during SL4 while the Y-3 detector array was in use in the S192 scanner. This mission was somewhat spontaneous and not thoroughly planned since the originally planned test site, Skaggs Hot Springs, California, was rejected at the last minute due to drift of the Skylab orbit. A preliminary helicopter overflight of The Geysers area at 1600 hours December 17 indicated that radiometric temperature differences on the order of 6°C did exist. Based on these encouraging data, a data gathering mission was planned to coincide with a predawn Skylab overpass (track 63, Pass No. 68, Rev. 3145) at 04:36 PDT December 18.

Two flight lines were flown at 5700 ± 500 feet A.S.L. or approximately 3500 feet (1070 meters) above mean terrain using the Barnes PRT-5. It was generally clear and the winds calm in The Geysers area. The following ground conditions prevailed: dry bulb temperature = 8.33°C, wet bulb temperature = 6.11°C, surface pressure = 712.5 mm of Hg (from U.S. Standard Atmosphere). The radiosonde data provided the temperature profile shown in Figure 3.6-1 and the humidity profile is shown in Figure 3.6-2. The water vapor concentration is shown in Figure 3.6-3.

The ground truth data acquired from the two flight-lines are graphically displayed in Figure 3.6-4. The insert (upper right) of this figure shows the location of a concentration of steam wells (near Geyser Canyon), Sulphur Creek, and the ridge crests on either side of Sulphur Creek. The dashed lines, labeled A-A' and B-B', indicate the approximate flight-line locations. It should be noted that there were few

reference points from which to judge aircraft location so that these flight lines may be mislocated by several hundred meters. Figure 3.6-4 also shows cross-sections along the flightlines. The solid line is a topographic profile (left scale is in feet above sea level) and the dashed line represents radiometric temperature (right scale is in degrees Centigrade). These data indicate that a rather broad area, containing the geothermal steam wells and steam power plants, had ground temperatures as much as 5 to 6°C higher than the normal forest and brush covered hills (background). It was decided that these profile data did not provide adequate control for the construction of an isothermal contour map. Also, there was some speculation that the higher temperature readings might be due to measuring hot pipes, power plants, and steam wells rather than actual ground temperatures.

3.7 January Daytime Mission Ground Truth Data - The second mission occurred on January 26, 1974 (track 63, Pass No. 91, Rev. 3173) at 12:41 PDT. The X-5 detector array had been installed in place of the Y-3 detector array used earlier in the S192 sensor. Extended helicopter flightlines were flown at an altitude of 4000 feet (1980 meters) ASL, about 2000 feet (625 meters) above mean terrain, during the time interval between 1300 and 1400 hours.

The atmosphere was clear with the following surface conditions: dry bulb temperature = 10.0°C, wet bulb temperature = 5.6°C, surface pressure = 718 mm of Hg, and wind = 3.5 mph from the north. The radiosonde data provided the vertical temperature shown in Figure 3.7-1 and the vertical humidity profile shown in Figure 3.7-2. The derived water vapor concentration is shown in Figure 3.7-3.

The data collected along five helicopter flightlines (shown in Figure 3.7-4) provided adequate data to plot generalized isotherms, especially in the immediate vicinity of The Geysers. In areas more remote from the flightlines, considerable "contouring license" was used. These data indicate a more complex thermal distribution than was suspected from the 18 December data. Instead of a large, generalized thermal anomaly, there appears to be several hot centers which make up a cluster pattern. Also, relatively warm areas exist beyond the currently developed area (notably to the northwest where temperatures reach 22°C). Because these are daytime acquired data, considerable variation can be expected from selective solar heating of topography. An example of this is the cool area to the north of The Geysers which coincides with a north slope. So-called "background" temperatures

seem to range from 6°C to about 18°C. Temperatures above 18°C may be associated with thermal anomalies. It is possible that the highest temperatures recorded (~26°C) are associated with hot hardware which are at temperatures around 100°C. The PRT-5 would integrate these high temperatures with the background surface temperature resulting in an intermediate reading.

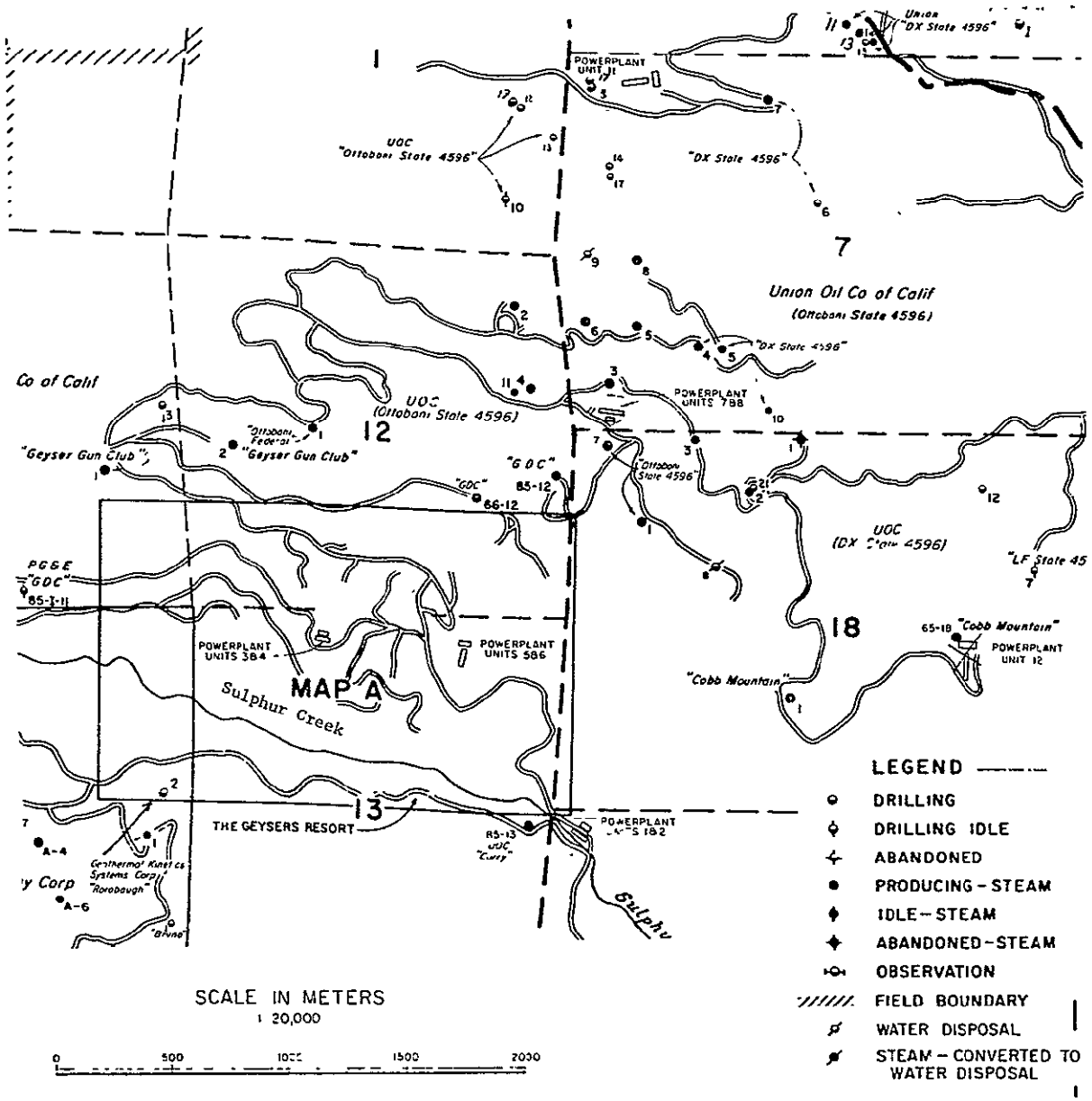

Figure 3.2-1 California Division of Oil and Gas Map Showing Location of Steam Wells and Power Plants. (From State of California, Division of Oil and Gas, 1416 9th St., Sacramento, California 95814, Map G6-1).

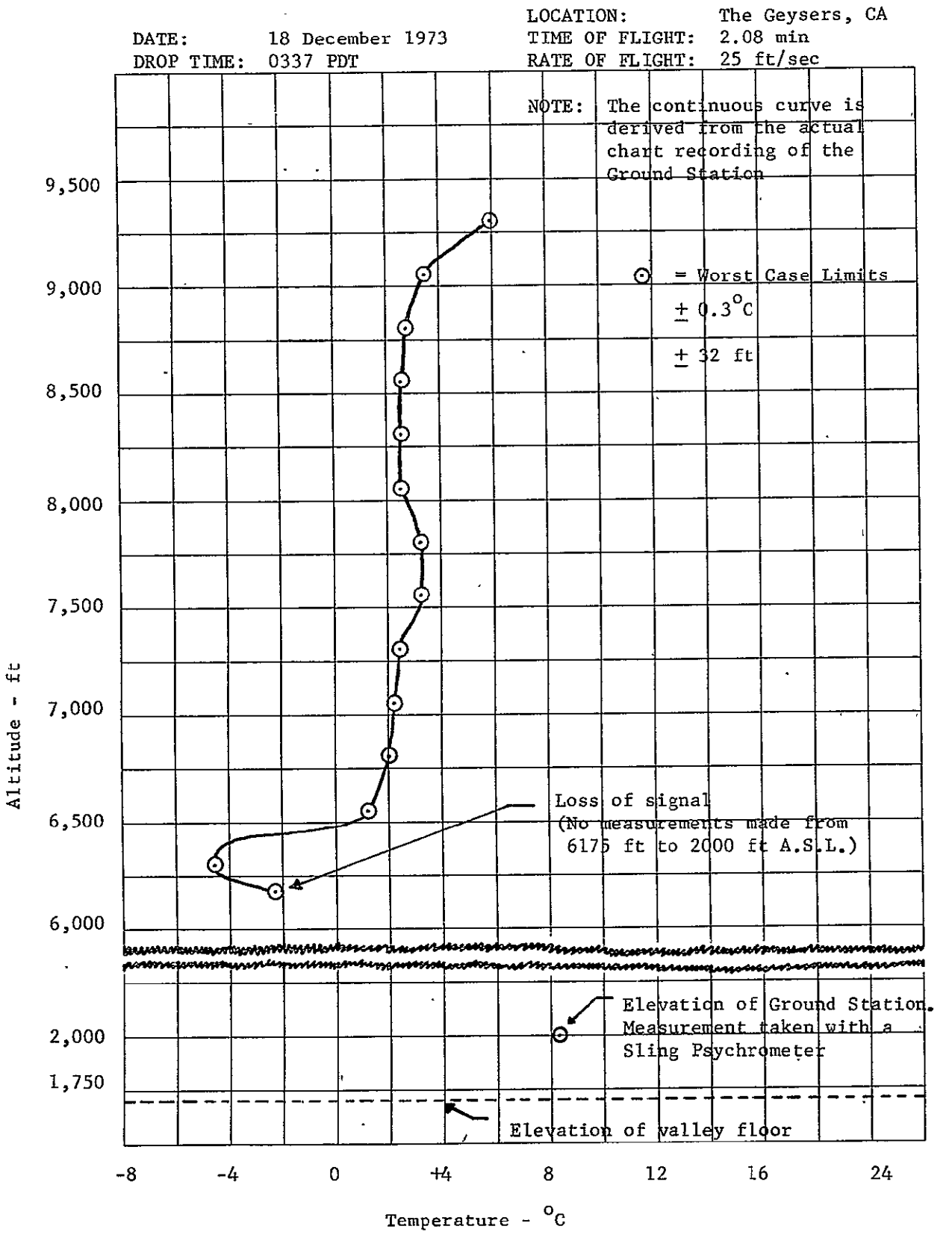

Figure 3.6-1 Radiosonde Temperature Profile for December 18, 1973

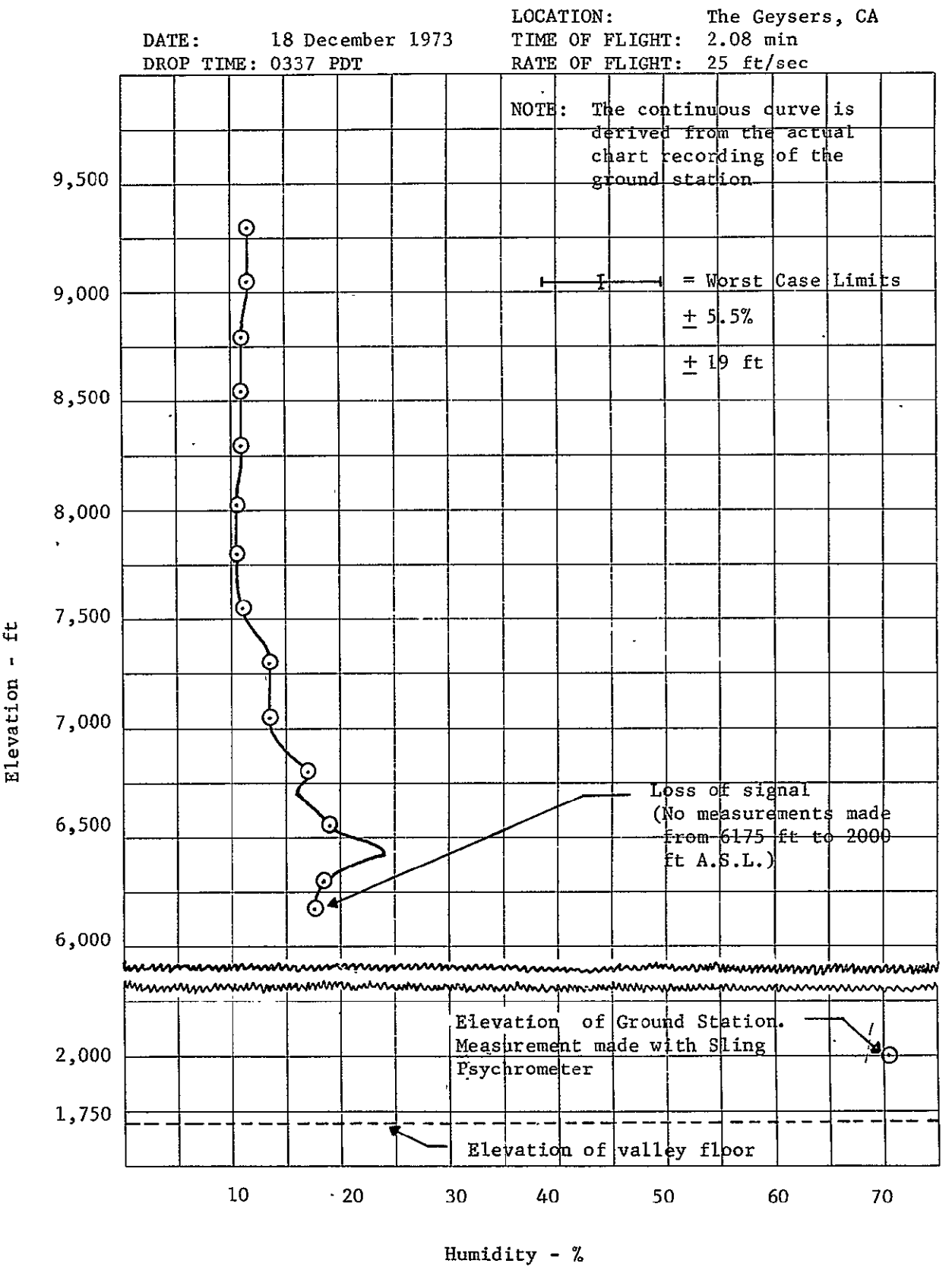

Figure 3.6-2 Radiosonde Humidity Profile for December 18, 1973

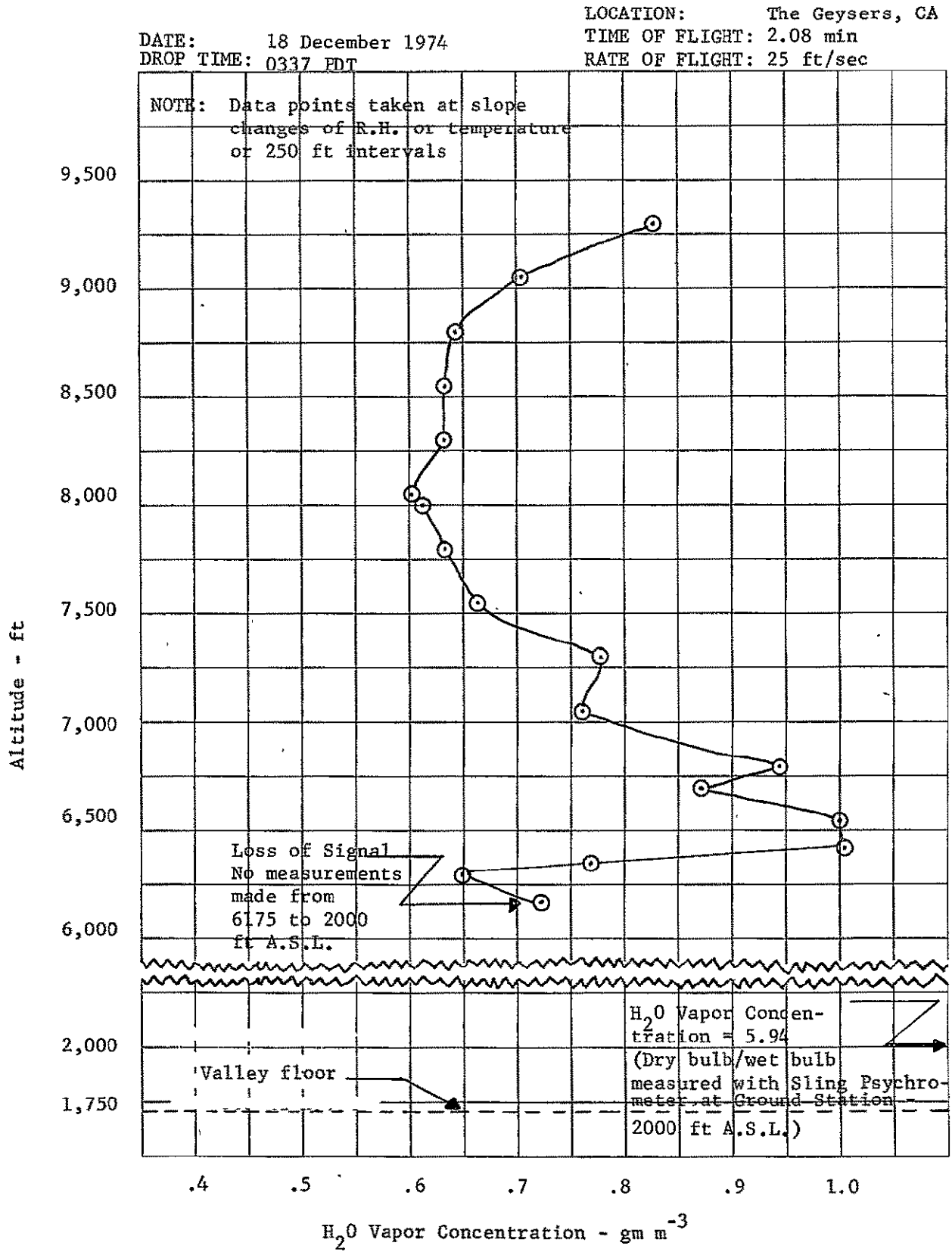

Figure 3.6-3 Derived Water Vapor Concentration for December 18, 1973

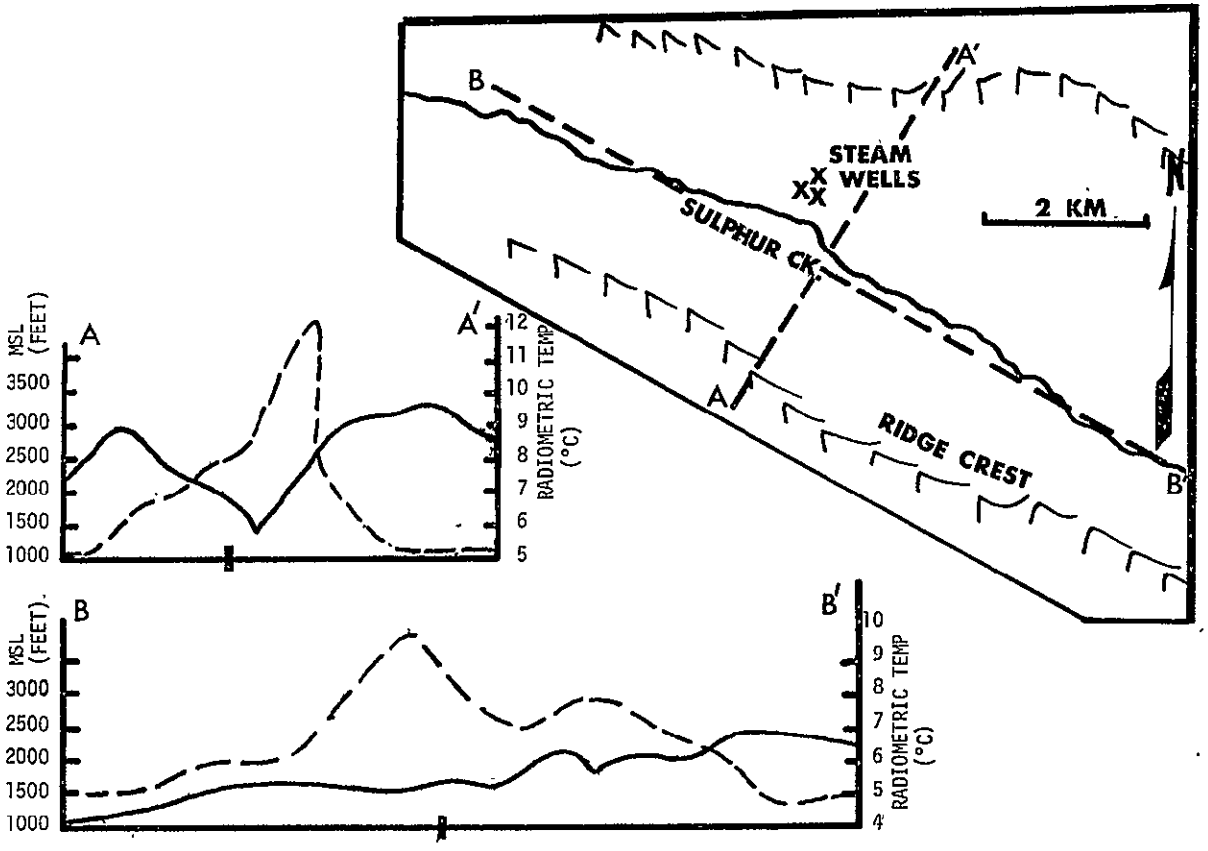

Figure 3.6-4 December 18, 1973 Ground Truth Data. Upper-right insert shows approximate location of flightlines relative to Sulphur Creek and ridge crests. The plotted curves are topographic (solid lines) and radiometric temperature (dashed lines) profiles along the indicated flightlines.

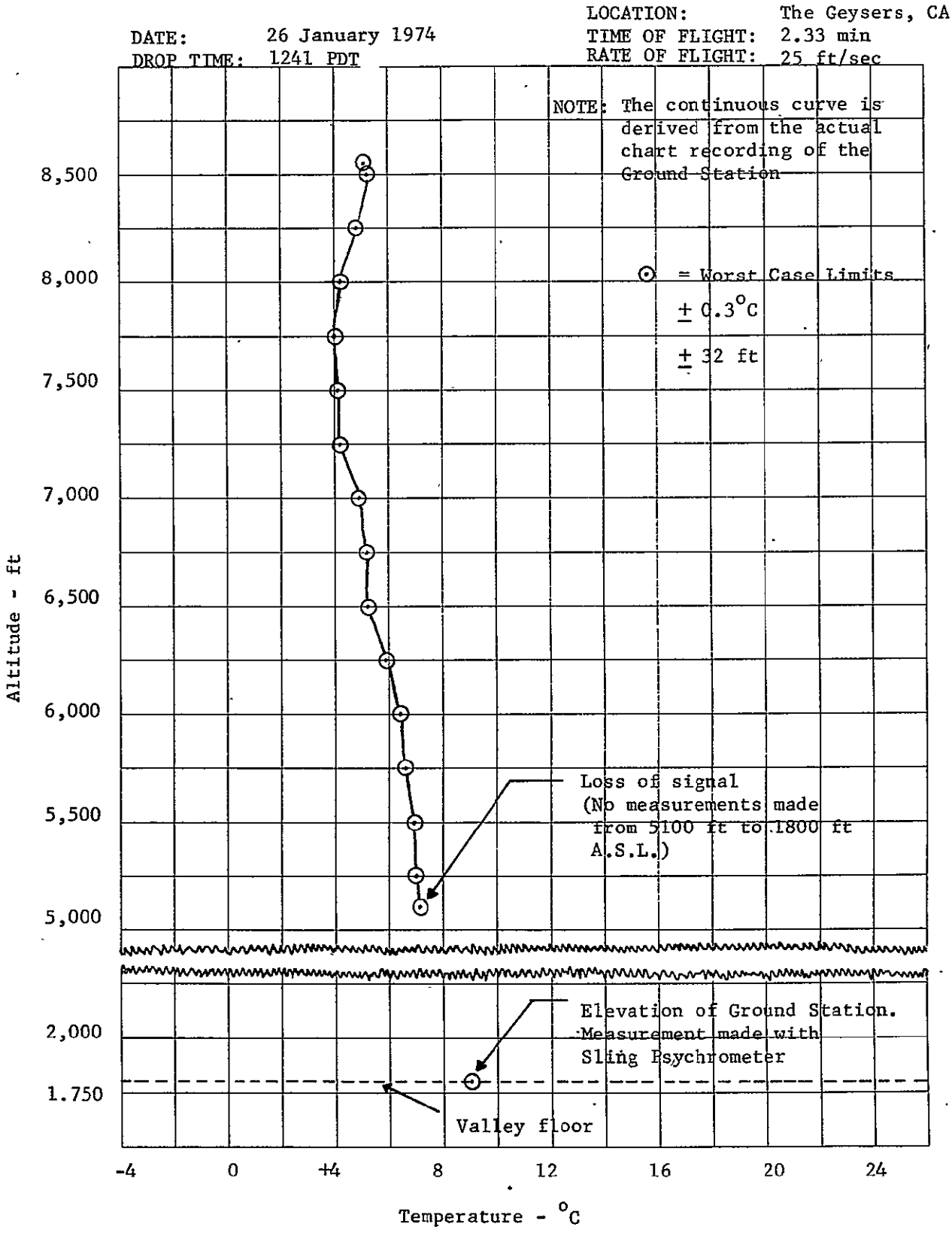

Figure 3.7-1 Radiosonde Temperature Profile for January 26, 1974

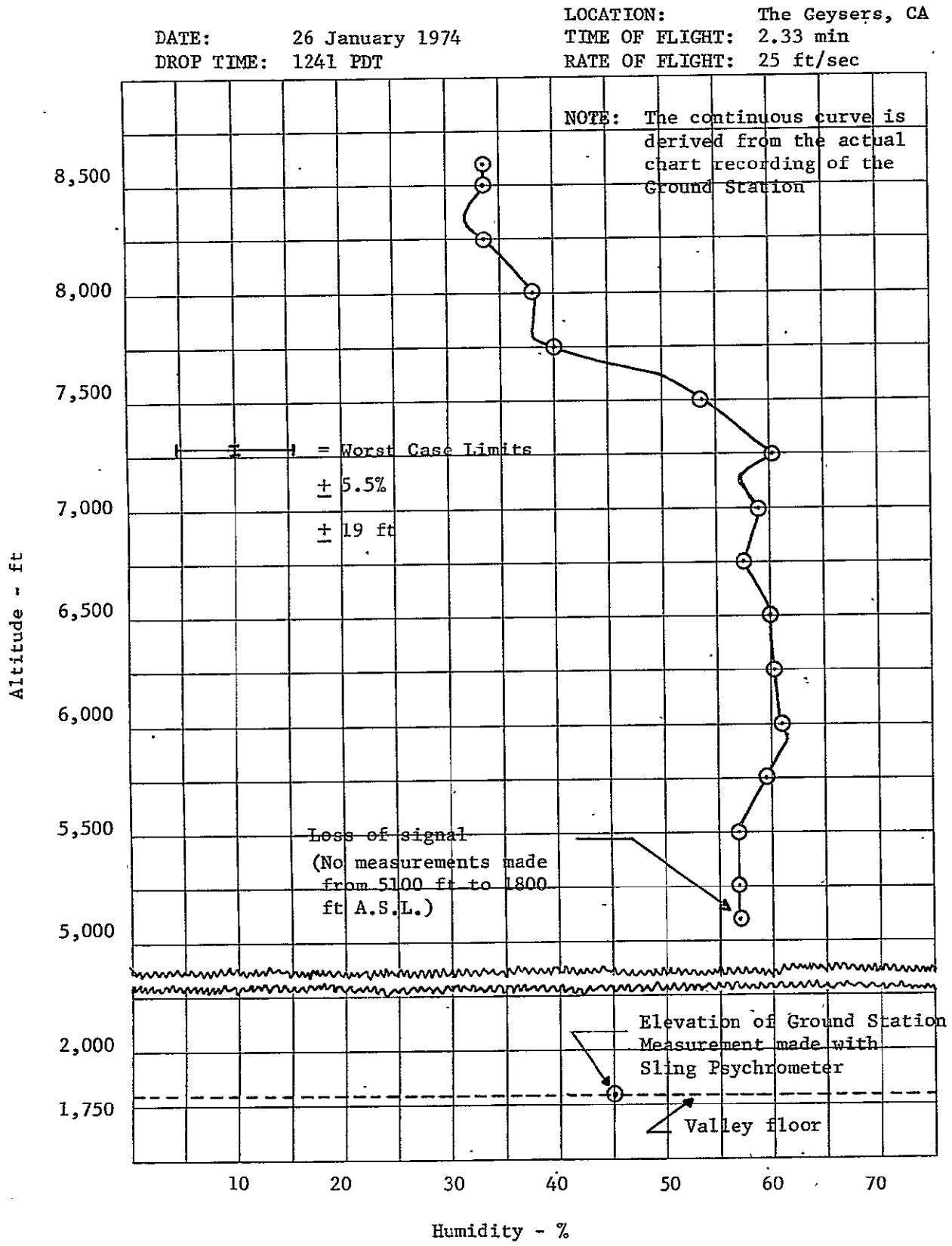

Figure 3.7-2 Radiosonde Humidity Profile for January 26, 1974

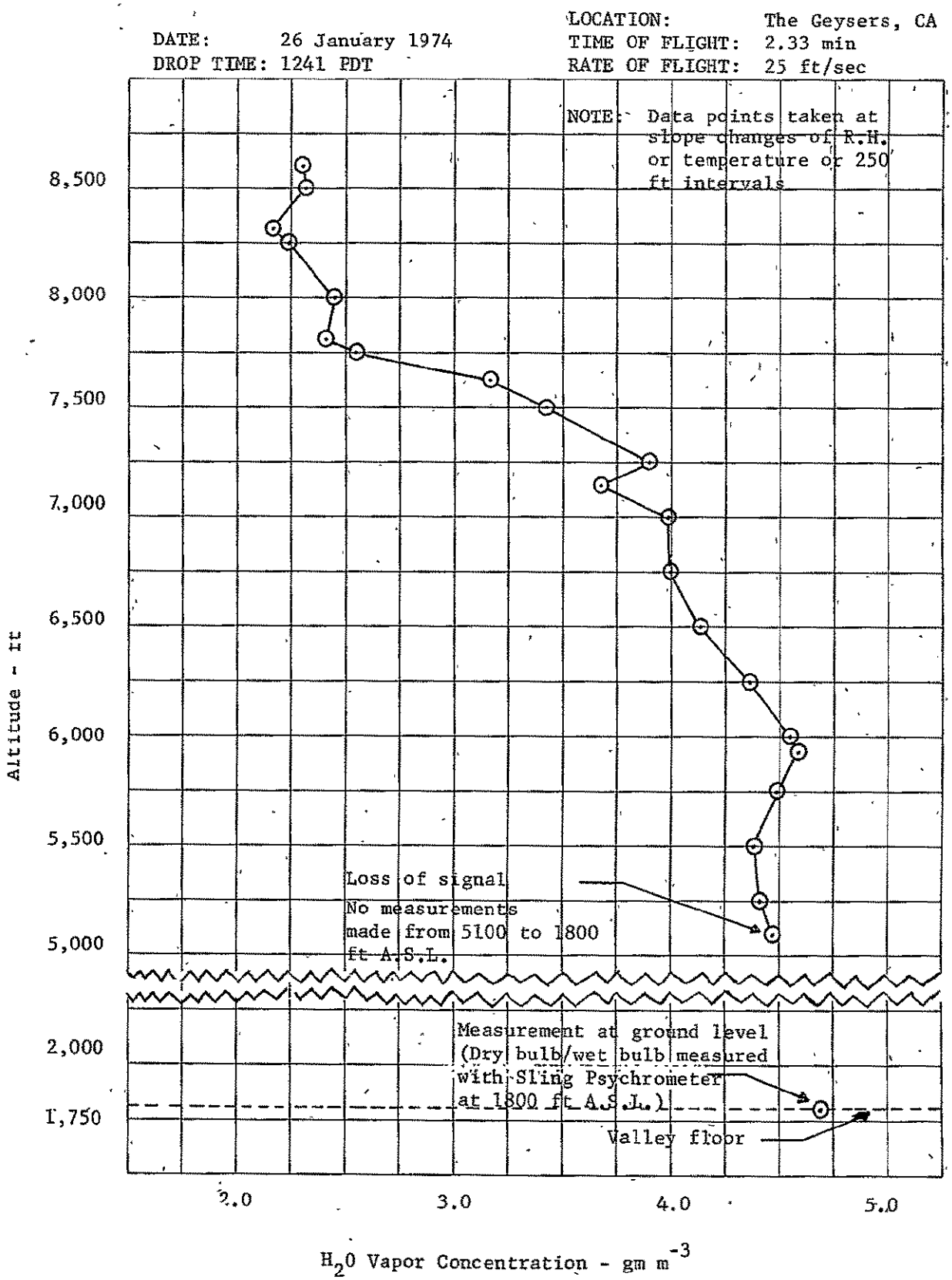

Figure 3.7-3 Derived Water Vapor Concentration for January 26, 1974

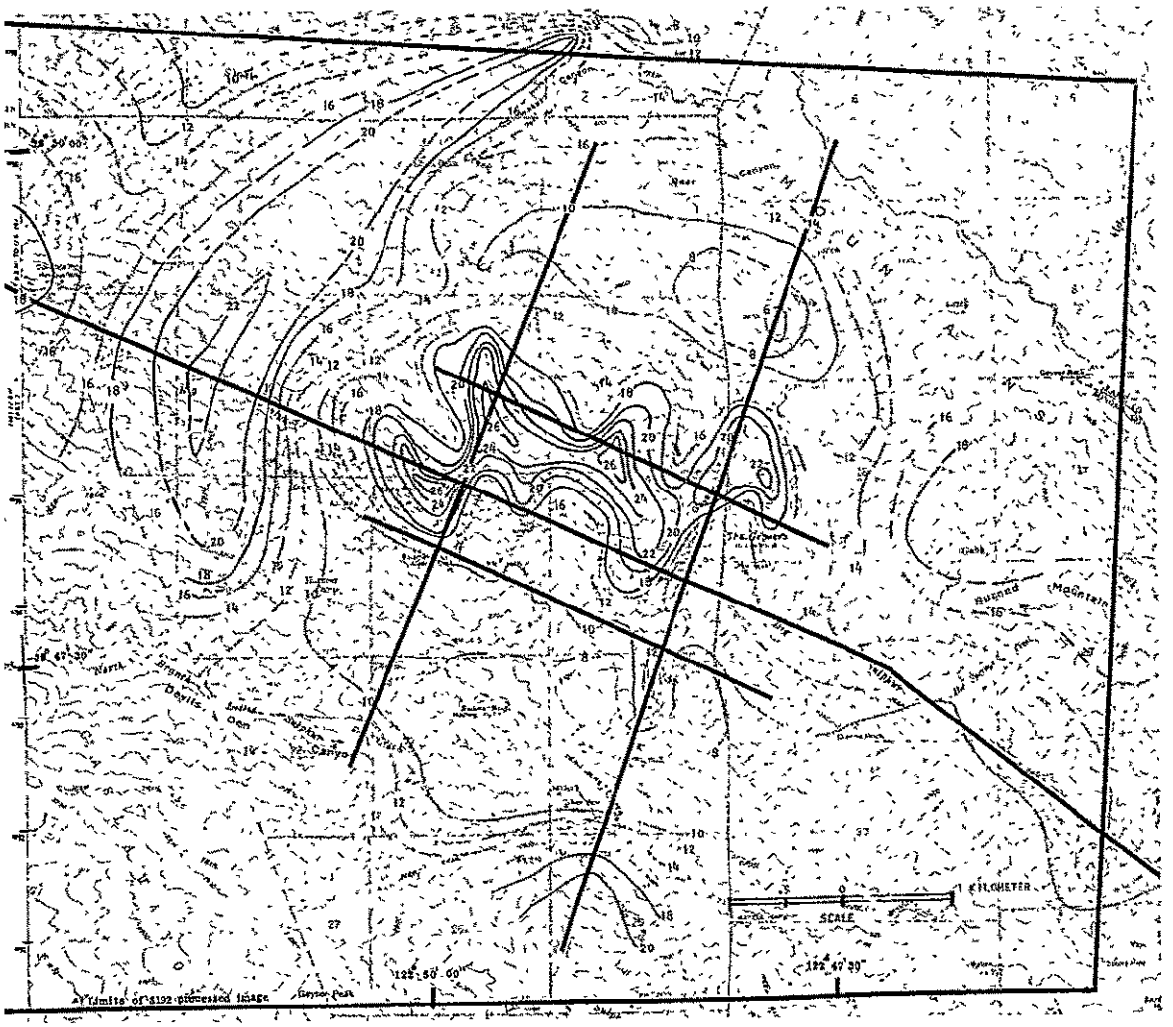

Figure 3.7-4 January 26, 1974 Ground Truth Data Overlayed on Topographic Map of The Geysers Area. Considerable "contouring license" was used in areas away from the indicated flightlines.

BAND	DESCRIPTION	RANGE (μm)	SAMPLES/SCAN
1	VIOLET	0.41 - 0.46	1240
2	VIOLET-BLUE	0.46 - 0.51	1240
3	BLUE-GREEN	0.52 - 0.56	2480
4	GREEN-YELLOW	0.56 - 0.61	2480
5	ORANGE-RED	0.62 - 0.67	2480
6	RED	0.68 - 0.76	2480
7	INFRARED	0.78 - 0.88	2480
8	INFRARED	0.98 - 1.08	1240
9	INFRARED	1.09 - 1.19	1240
10	INFRARED	1.20 - 1.30	1240
11	INFRARED	1.55 - 1.75	2480
12	INFRARED	2.10 - 2.35	2480
13	THERMAL INFRARED	10.2 - 12.5	2480/1240

TABLE 3.4-1 Spectral Band Coverage

4. DIGITAL PROCESSING DESCRIPTION

4.1 Image Processing Facility - The S192 scanner data of The Geysers area exists as a computer compatible digital magnetic tape for the two EREP passes mentioned. A computer facility capable of photographic data display was employed to form images and contour maps of The Geysers area. This facility produces black and white slow scan images which were photographically recorded. Except for the image forming capability, the computer is a standard medium sized computational facility with perpherals such as disc storage, a magnetic tape unit, line printer and card reader. The facility has 65K of core and uses 16 bit words. Fortran and assembler software are available. For image operations, a special software package was used which makes interactive image command convenient. See Appendix A for further discussion of the facility and related software that was developed under a Martin Marietta independent research and development task.

4.2 Image Processing Software - For the S192 data, a tape editing routine was established which selected the desired multispectral data of interest from the larger volume of unwanted digital tape data. Figure 4.2-1 shows the results of the area and scale selection capabilities of this routine. The desired data was converted to standard picture format for the Martin image processing software system (see Appendix A) and placed in magnetic disc storage. This image software system supplied the needed functions such as histograms, statistics, disc and display peripheral control and many other support functions necessary for image processing. Specific additions for handling S192 data were made to the image software system to perform area selection, geometric correction, digital enlargement, contour maps, calibration, filtering, average offset correction, and a moving average differential and calibrated offset correction. The contour algorithm used the method of significant bit truncation to produce level sliced contours. Details of the calibrated differential offset routine are presented in Appendix B. All programming was done in SEL-72 assembler language. Some of the important algorithmic principles are shown in the following processing discussion.

A. Overview of California Coast

B. Upper Left Quarter of Overview

FIGURE 4.2-1 The Geysers Site Location by Using Band 11 on X-5 Day Tape

5. DIGITAL PROCESSING DISCUSSION

5.1 Basic Processing Sequence - The sequence of algorithmic operations on the edited disc files of thermal data will be presented by example.

Figure 5.1-1 shows the first order geometric correction applied to both the X-5 and Y-3 data before further operations. This was done by digital interpolation and data translation on a line by line basis. Next, digital enlargement and area selection was applied as shown in Figure 5.1-2.

Figure 5.1-3A shows that the resulting data did not produce a good contour map. The image is too busy with detail and perhaps noise. Part of the difficulty was that the level slicing nature of the contour algorithm required that each contour level be occupied by image values in order that the contours be connected. Processing was necessary to provide connected data behavior by interpolation or smoothing. Figure 5.1-3B shows the contour result when a smoothing algorithm was applied. The smoothing filter shown in Figure 5.1-4 took the pixel in question plus the four surrounding pixels for inputs to an average value which replaced the center pixel value in the output image. One application of this algorithm was not adequate. The smoothed data contour map in Figure 5.1-3B used five successive applications of this smoothing algorithm.

The contour algorithm provided a non linear and periodic assignment of display output intensities to input pixel levels as shown in Figure 5.1-5. Such a mapping provided an expanded dynamic range of levels and an exact calibration of the resultant image independent of photographic operations after the display.

Two principal display assignment methods were employed as shown in Figures 5.1-5A and 5.1-5B. In Figure 5.1-5A, increasing lighter shades of gray are assigned to increasing temperatures in a "stairstep" manner over the interval 0 to 3.5°C. But at 4°C, the output tone becomes black again and starts another cycle which increases to 7.5°C. Thus, 0°C, 4°C, 8°C, 12°C, and 16°C are black and 3.5°C, 7.5°C, 11.5°C and 15.5°C are white. 2°C, 6°C, 10°C and 14°C are gray. If the data are sufficiently smooth as in Figure 5.1-3B, then it is possible to determine the direction of increasing temperature anywhere on the output image. If the temperature at any point in the map is known, then the number of cycles and direction can be counted and the temperature at any other point determined.

If the display method of Figure 5.1-5B is used, then a more conventional contour map results but the contours have to be labeled by another process external to the algorithm.

The contoured display methods require that values exist at each level in Figure 5.1-5 in order for a well behaved map to result. In other words, the data has to be continuous or smooth. Figure 5.1-3A is an example of results without suitable smoothness. Since the S192 thermal band unfiltered data contain so much variation, due to ground thermal variation and/or noise, all of the following thermal contour images have received five applications of the smoothing algorithm shown in Figure 5.1-4.

5.2 Y-3 Data Processing Difficulties - One cheif objective of this investigation was to compare the capabilities for producing thermal images of the S192 data taken with the Y-3 and X-5 detector arrays. As can be seen in Figure 5.2-1, the Y-3 data presented processing difficulties. In contrast the X-5 data required no special image processing to produce excellent quality thermal images. Since most of the S192 data were taken with the Y-3 detector array, there was good reason to develop image processing which would improve the quality of images produced from Y-3 data.

The image produced from the raw Y-3 data is shown in Figure 5.2-2A. The first attempt to improve the image quality resulted in the thermal image in Figure 5.2-2B. This was the result of applying the calibration equation

$$\text{OUTPUT} = \frac{\text{RAW} - \text{LOW}}{\text{HIGH} - \text{LOW}}$$

Where HIGH and LOW denote the average of the six data values for the high and low temperature calibration sources, RAW is the raw data value, and OUTPUT is the displayed function.

Next, an offset from the full scan line scenic mean correction produced the image shown in Figure 5.2-3B. The image resulting from the calibration equation above is shown for comparison in Figure 5.2-3A. An application of the offset from the full scan line scenic mean correction produced the image shown in Figure 5.2-4A which has been enlarged and smoothed with the spatial filter of Figure 5.1-4. The improvement was not good enough for contour mapping purposes. The residual streaking was from a more rapid offset drift occurring within

each scan line. Additional improvement was obtained from an offset from a more local scan line segment, instead of the full scan line, scenic mean. Figure 5.2-4B used a 255 pixel scenic mean covering the region of the area selected offset correction. The improvement indicated that offset drift within a scan line could be filtered out by a method which dynamically tracks the scenic mean within a scan line.

5.3 Local Differential Offset Algorithm - A refinement of the dynamic local segment method of the last section resulted in the images shown in Figure 5.3-1B and 5.3-2B. Figure 5.3-2 is an enlarged image. The improved quality of these images was sufficient to permit the production of usable thermal contour maps. The raw count for each point was dynamically corrected by a difference of two local moving averages which detects local offset drift error. Each pixel was then calibrated by centered moving averages of the high temperature and low temperature calibration sources.

Figure 5.3-3 shows the local differential offset scheme. The raw count $C_{X_0 Y_0}$ at G was modified by the difference between the averages $T_{X_0 Y_0}$ and $S_{X_0 Y_0}$. This average difference detected how much the scan line $\overline{AF}$ had faded or intensified compared to all the scan line segments contained in CDEF. Since G was central to CDEF and centered moving average modifications were made each time G was moved, this process sufficed to track dynamically offset fading both within a scan line and between scan lines. This operator was much more local and dynamic than any of those previously employed. H_{X_0} and L_{Y_0} were centered moving averages of the high temperature and low temperature calibration sources.

33 scan lines and 33 pixels were used in application of the local differential offset algorithm. A detailed description of the implementation of this algorithm is presented in Appendix B. The power of this algorithm is illustrated by the comparison of the two thermal contour maps in Figure 5.3-4.

5.4 Contour and Threshold Maps - Figures 5.4-1 to 5.4-6 are examples of the daytime and nighttime thermal contour maps which were produced from the S192 multispectral scanner. Figure 5.1-5A applies to stairstep contours and Figure 5.1-5B applies to outline contours except for the contour interval.

A color display could be used to overlay more than one image output such as contours of the original data and candidate

sites. Color digital processing would give the human user three times the data in one image when compared to black and white. We have achieved almost as much as could be gained by color techniques by using multiple image black and white comparisons external to the system. The reason for using black and white was the fact that we have a working black and white processing system ready to evaluate quickly in high volume the various questions regarding the X-5 and the Y-3 data and to produce color would have involved a considerable delay in our output and conclusions. The timely answers provided about the various processing techniques attempted could not have been obtained if emphasis has been given to color outputs.

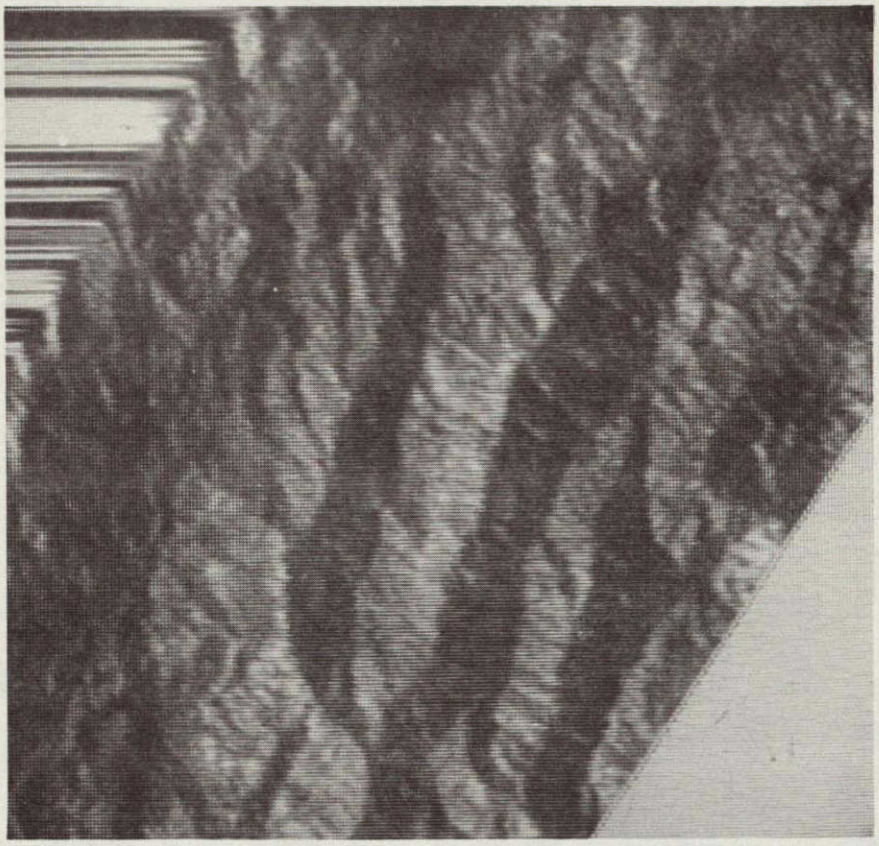

B. X-5 Geometrically Corrected

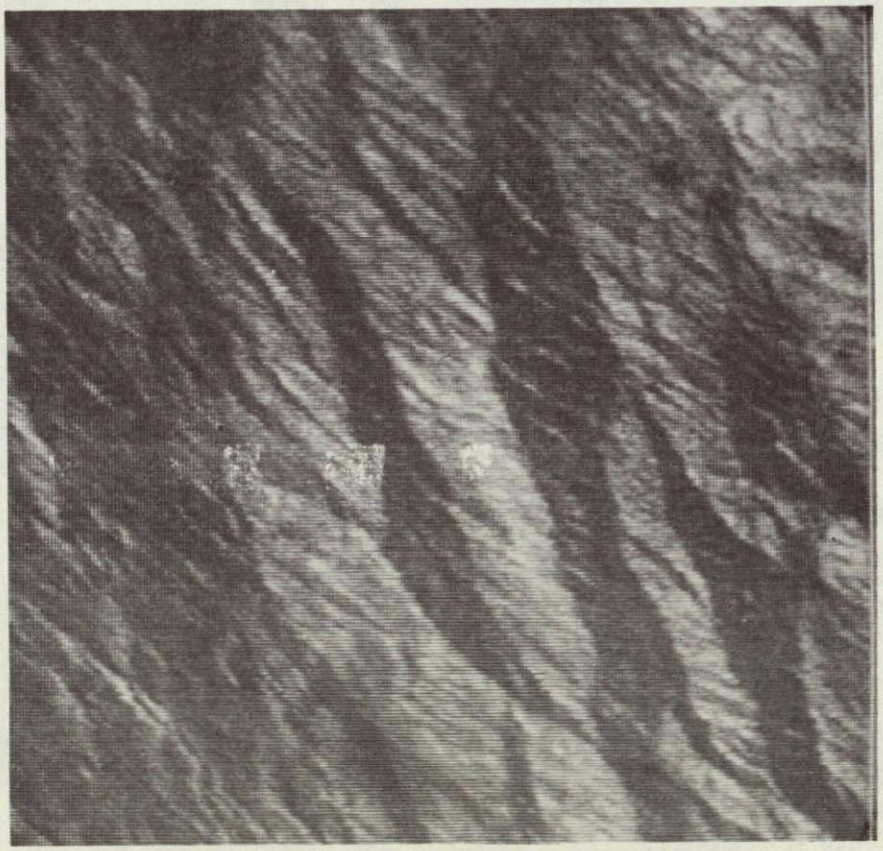

A. X-5 Original

FIGURE 5.1-1 First Order Geometric Correction

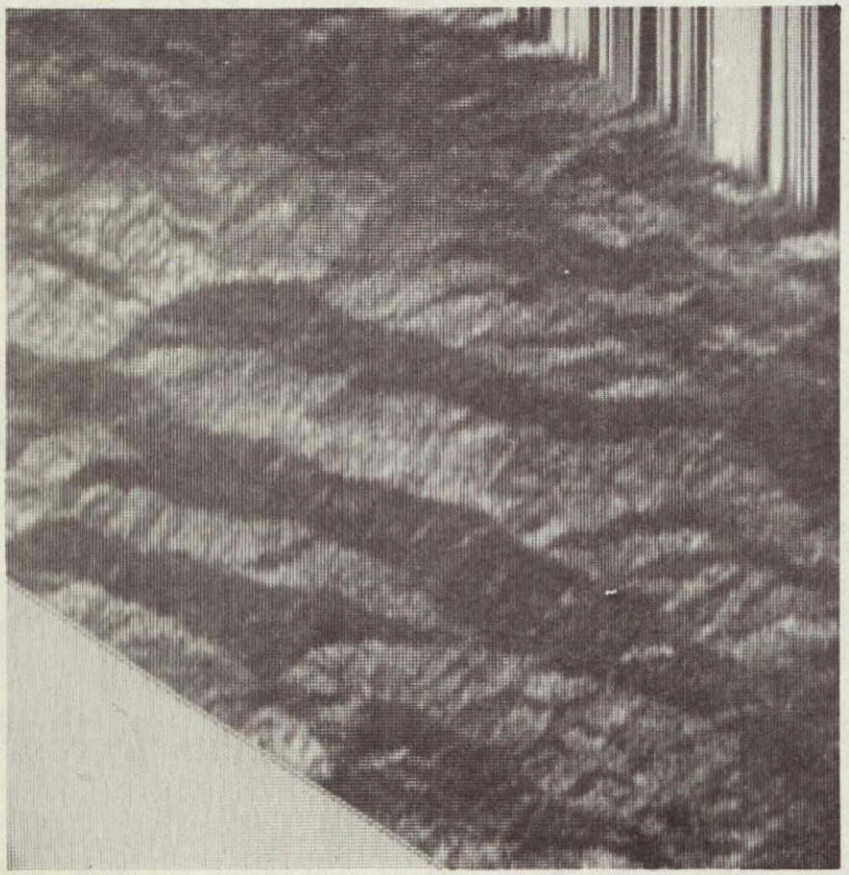

A. X-5 Original Geometrically Corrected

B. X-5 Enlargement (Times Two)

FIGURE 5.1-2 Digital Enlargement and Area Selection

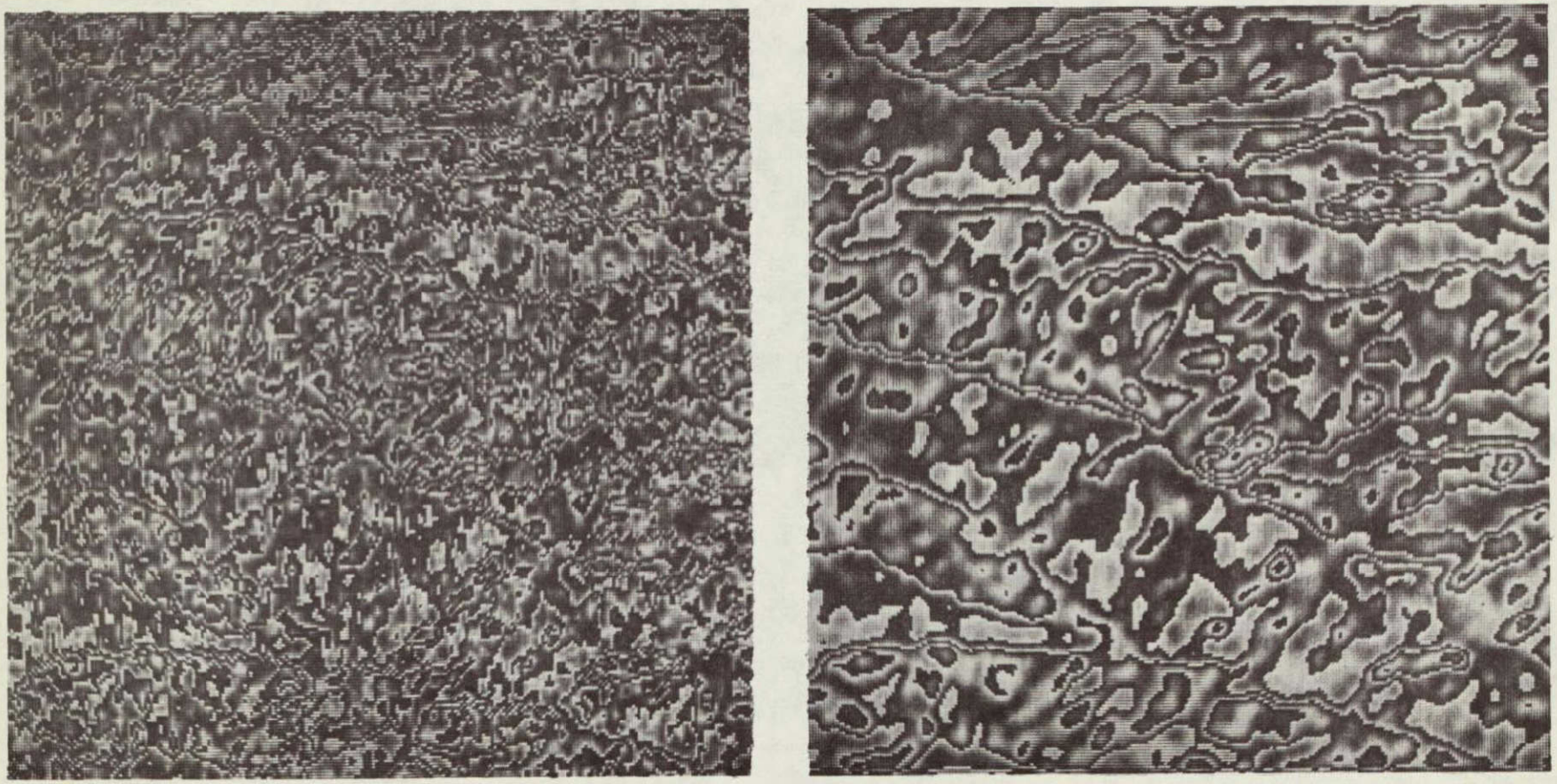

A. Contours on Unsmooth Data

B. Contours on Smooth Data

FIGURE 5.1-3 Smooth Data Requirement

MSC-05538

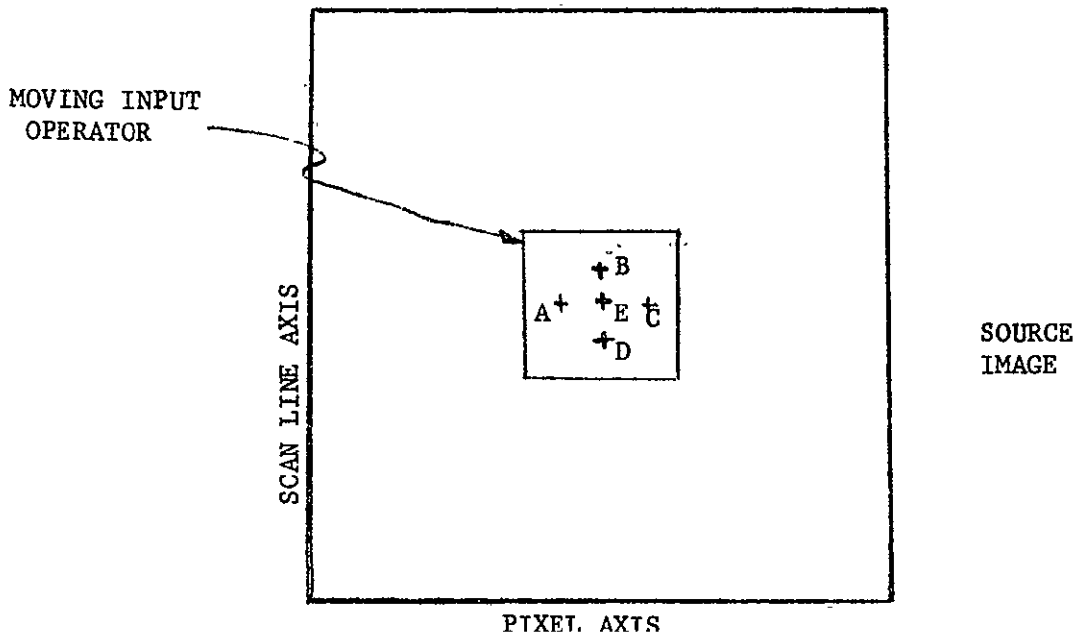

$$E' = \frac{A + B + C + D + E}{5}$$

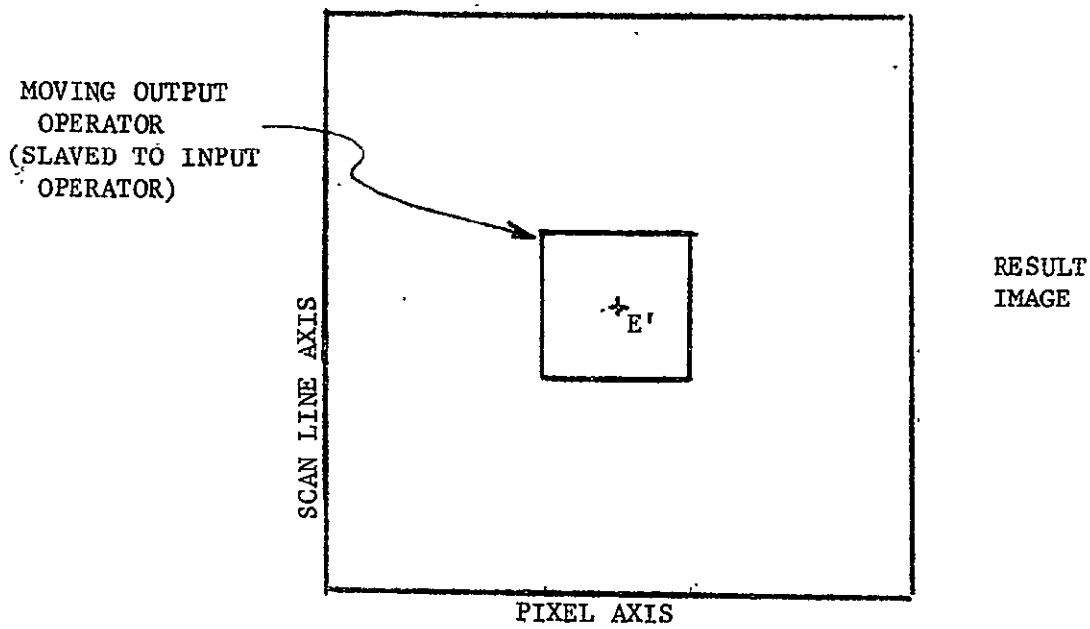

FIGURE 5.1-4 Smoothing Algorithm

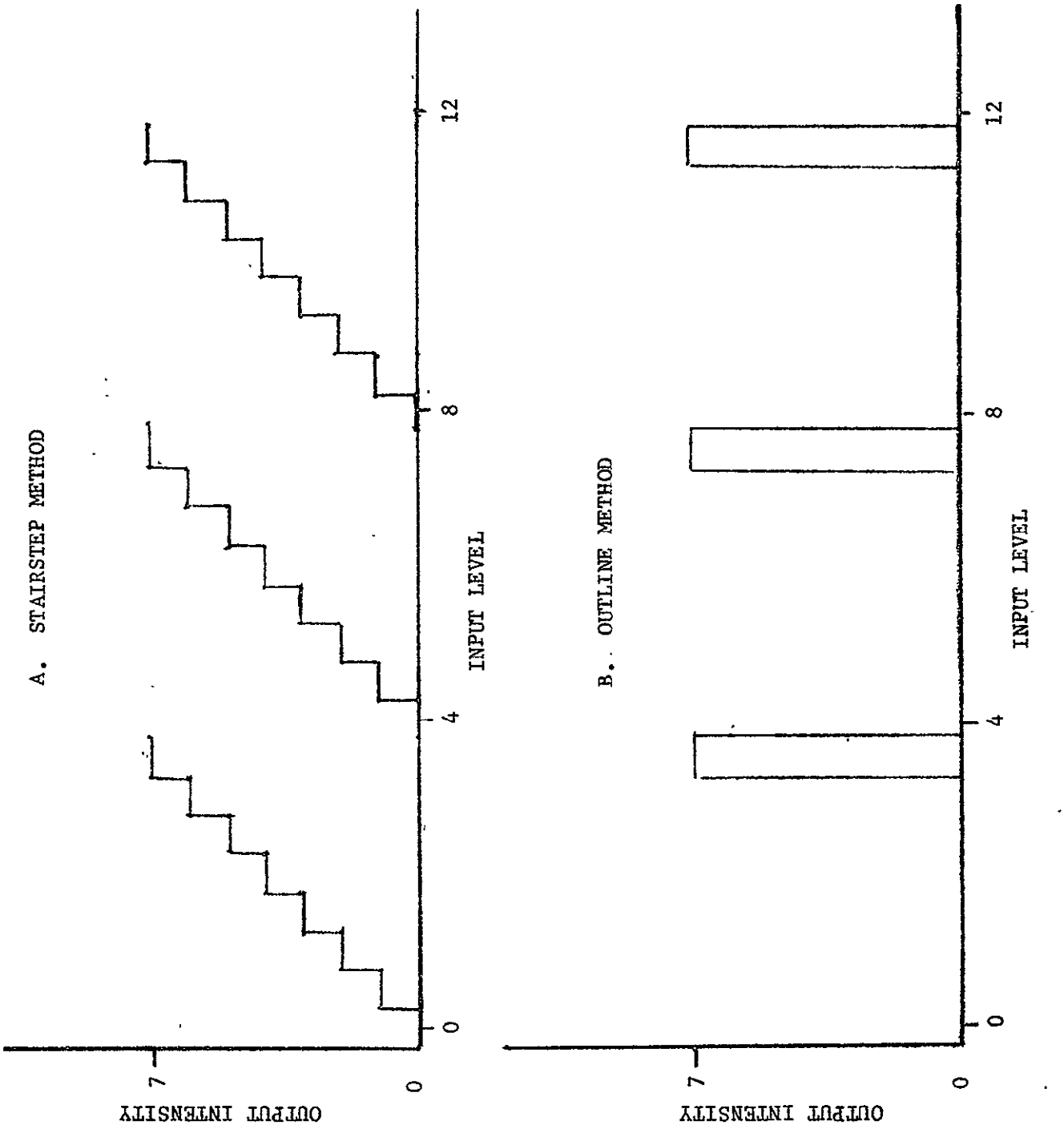

FIGURE 5.1-5 Contour Map Transformation

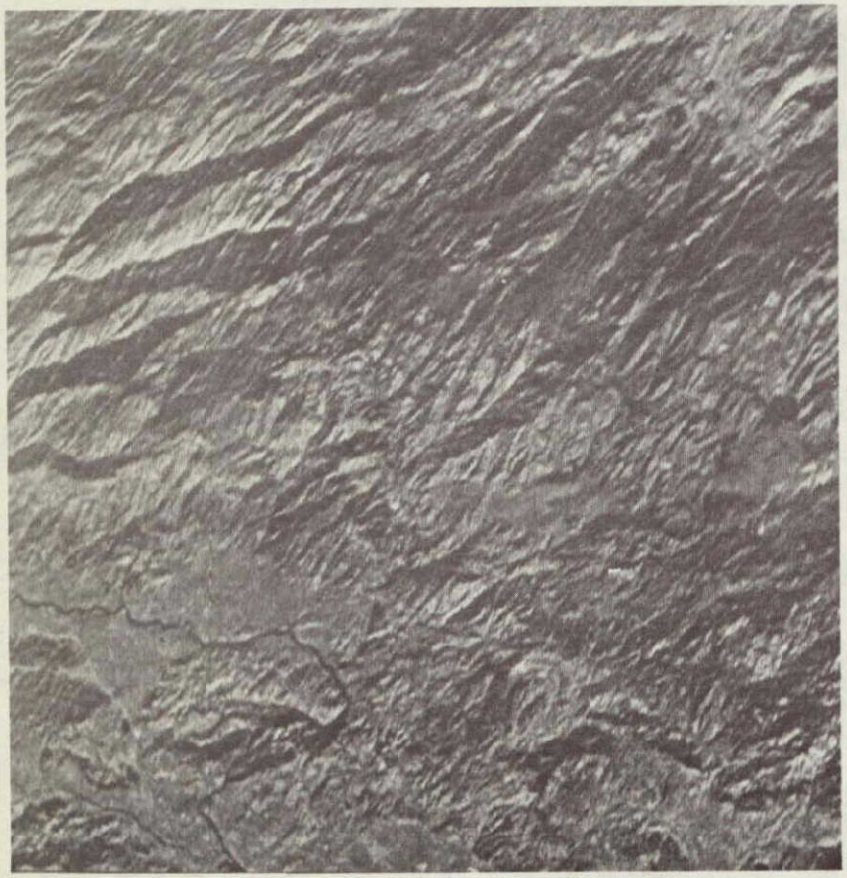

A. X-5 Day Pass

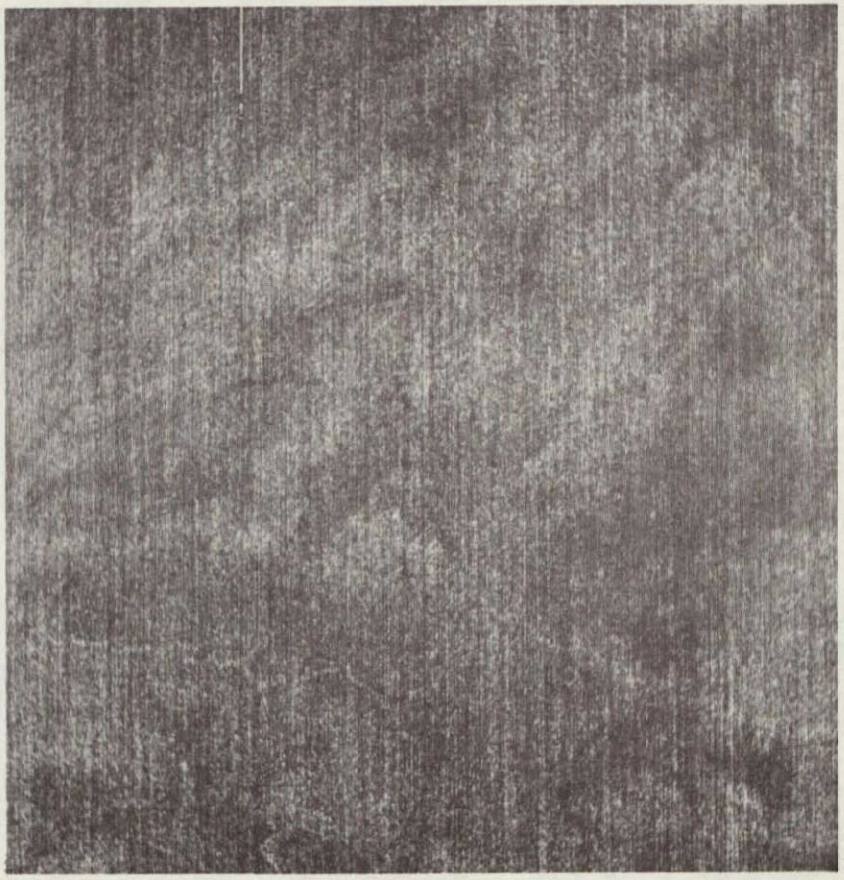

B. Y-3 Night Pass

FIGURE 5.2-1 Comparison of X-5 and Y-3 Data Over the Russian River and The Geysers

A. Raw Y-3

B. Calibrated Y-3

FIGURE 5.2-2 Calibration Problem with Y-3 Data

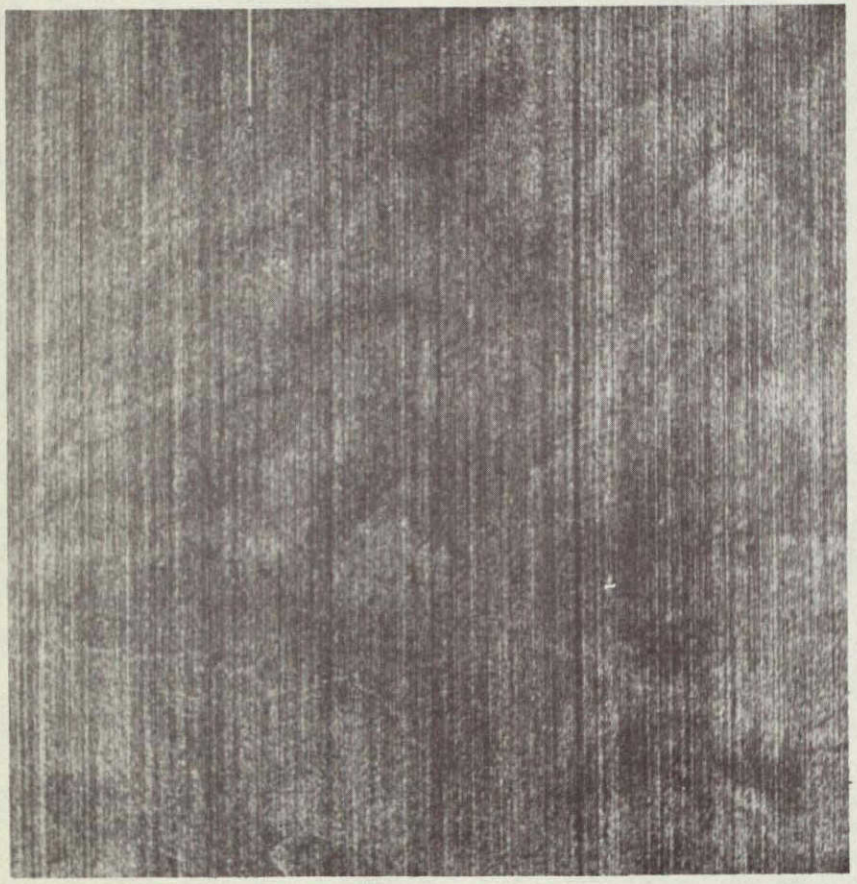

A. Standard Calibration

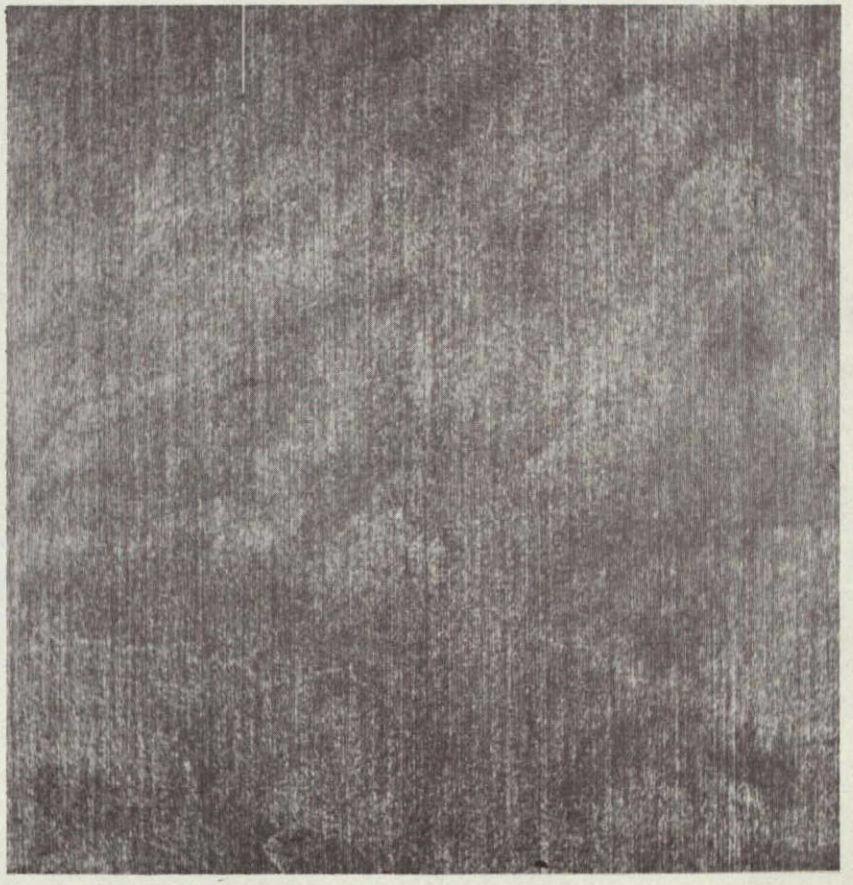

B. Offset from Scenic Mean

FIGURE 5.2-3 Improvement of Y-3 Data

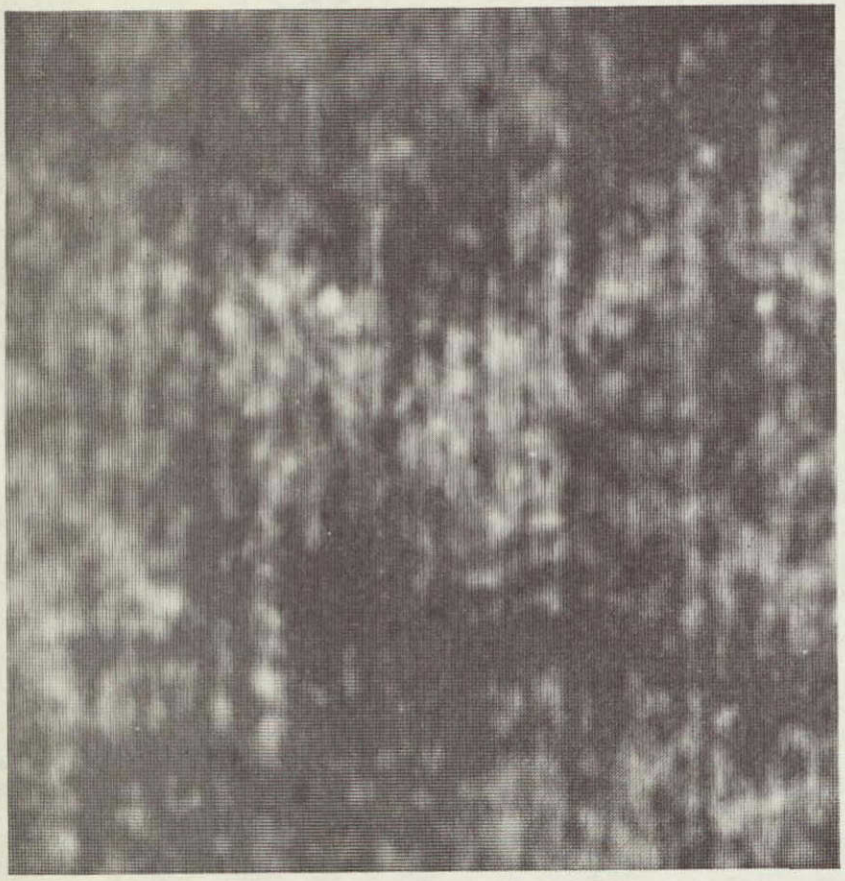

A. Offset from Full Scan Line Scenic Mean and Filter

B. Offset from Local Segment Scenic Mean and Filter

FIGURE 5.2-4 Further Improvement of Y-3 Data for Contour Map

A. Offset from Full Scan Line Scenic Mean and Filter

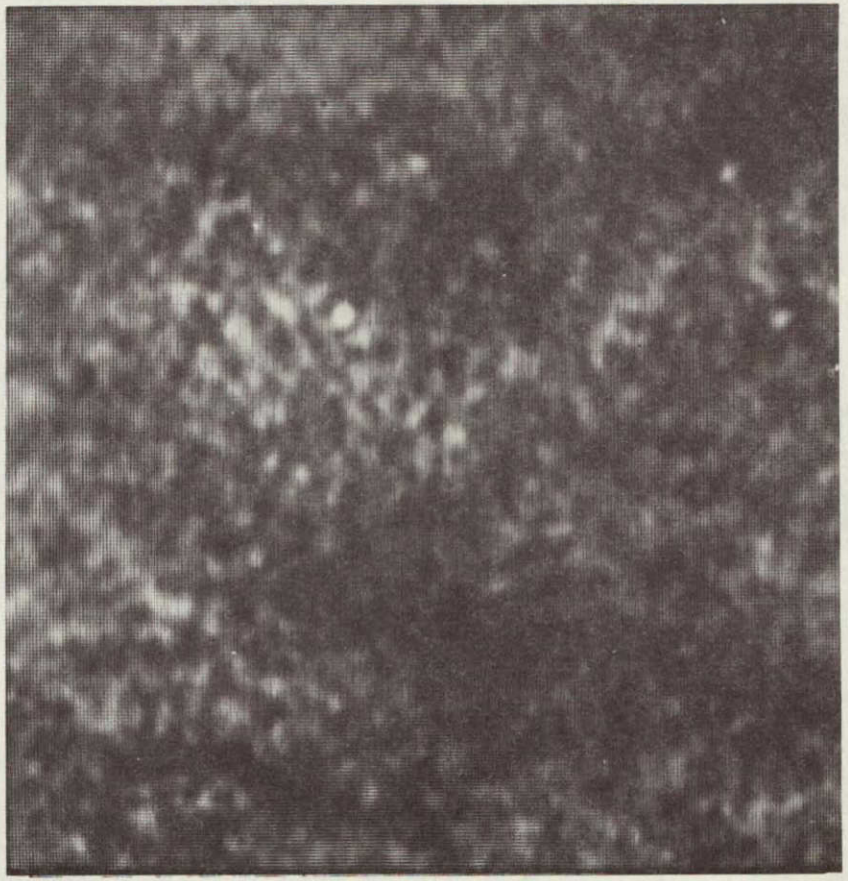

B. Calibrated Local Differential Average Offset and Filter

FIGURE 5.3-1 Further Improvement of Y-3 Data

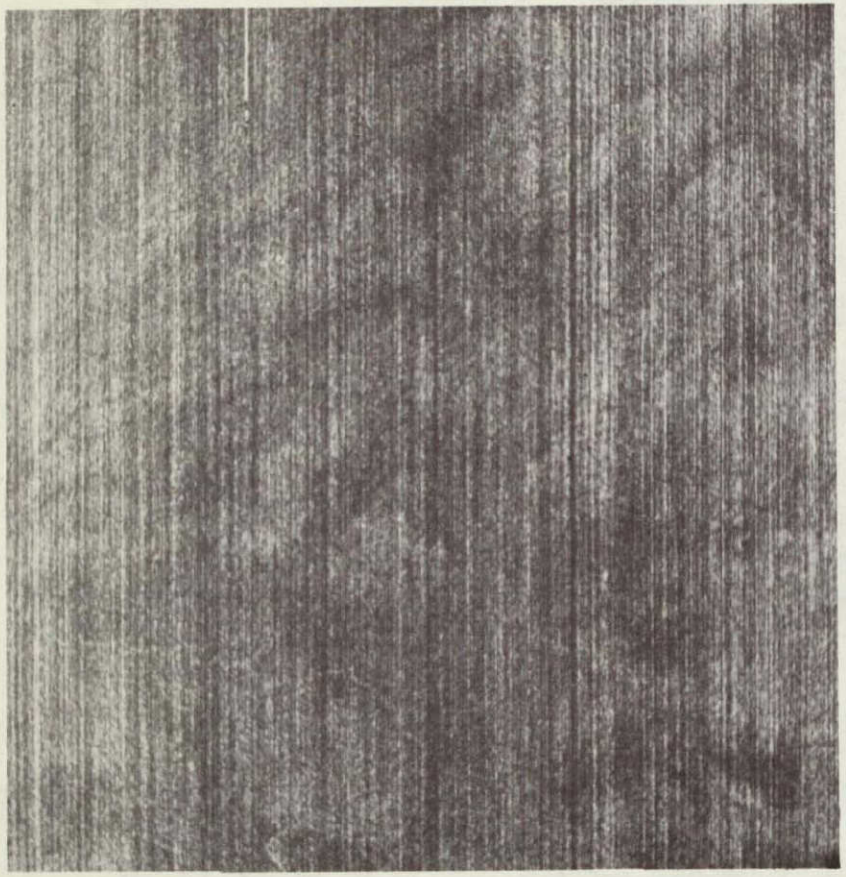

A. Standard Calibration

B. Calibrated Local Differential Average Offset

MSC-05538

FIGURE 5.3-2 Improvement of Y-3 Data

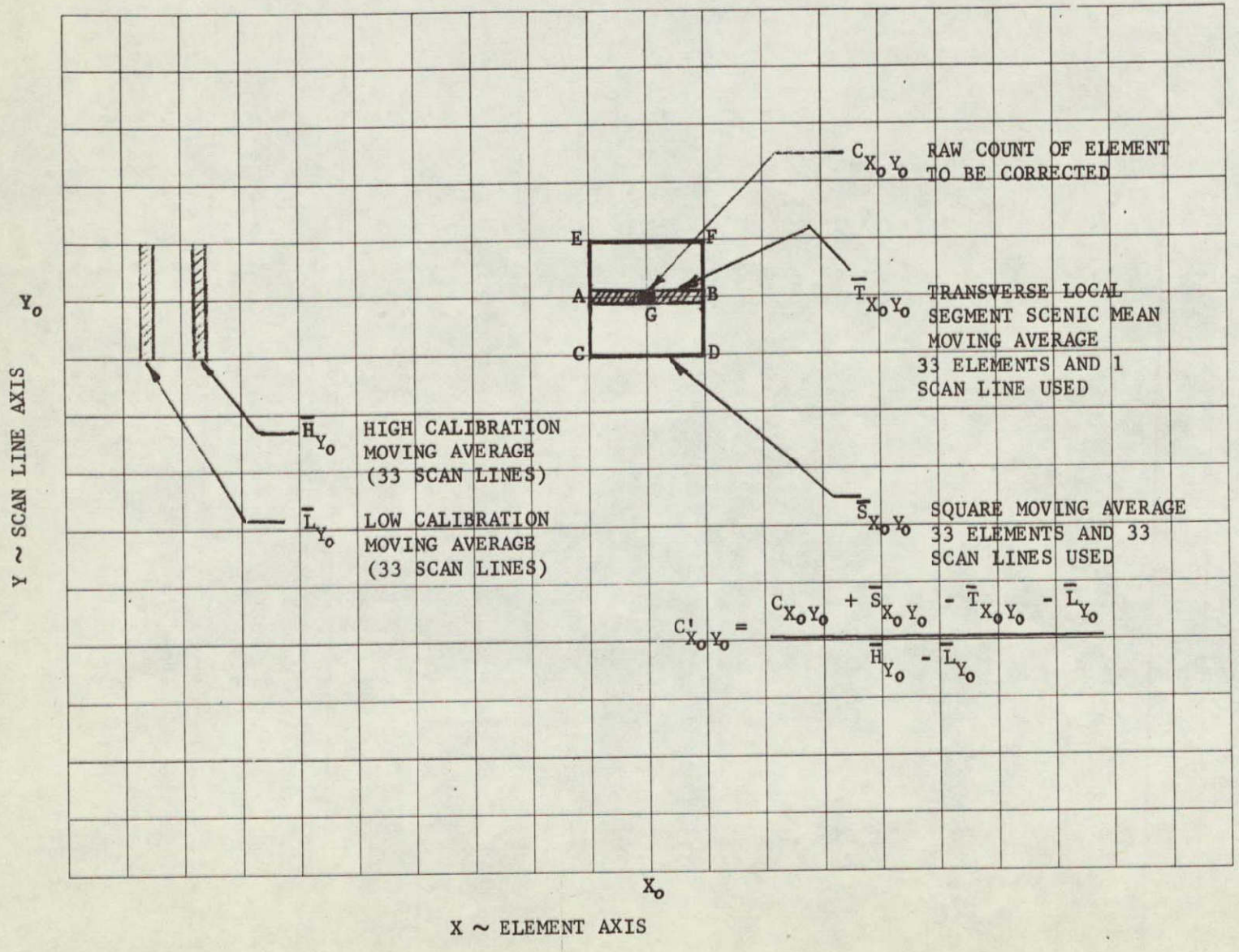

FIGURE 5.3-3 Calibrated Local Segment Differential Moving Average Correction

A. Full Scan Line Scenic Mean Correction

B. Calibrated Local Differential Average Offset Method

FIGURE 5.3-4 Comparison of Contour Maps from Full Scan Line Mean Correction and Local Differential Offset Correction

MSC-05538

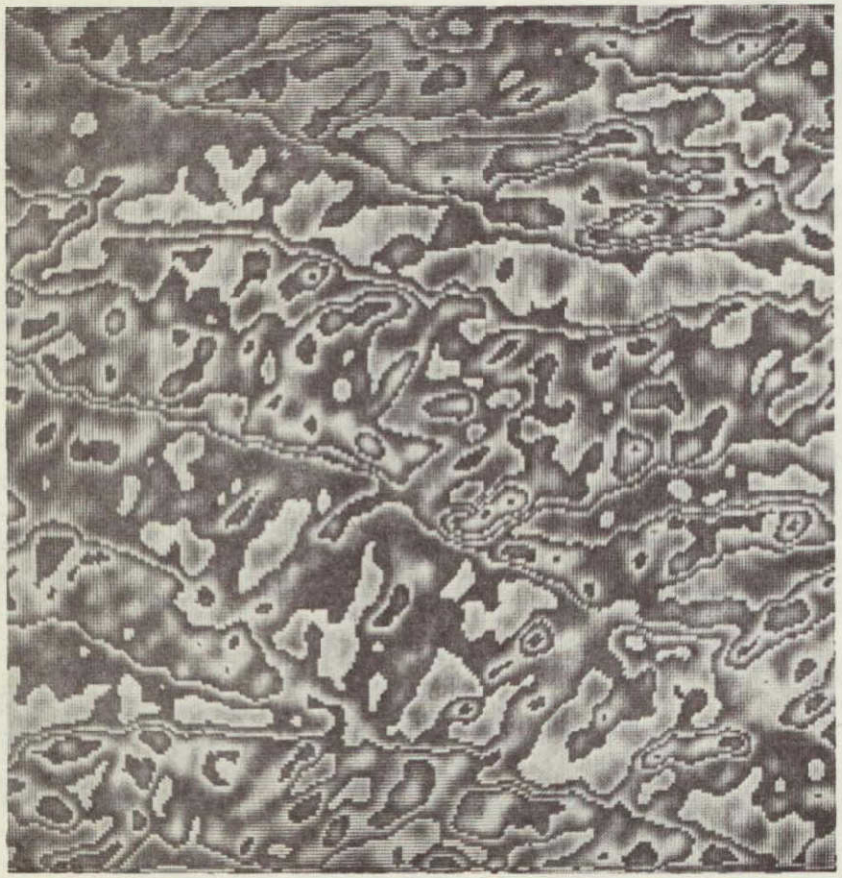

A. X-5 Contour Map (4°C Interval) (Day)

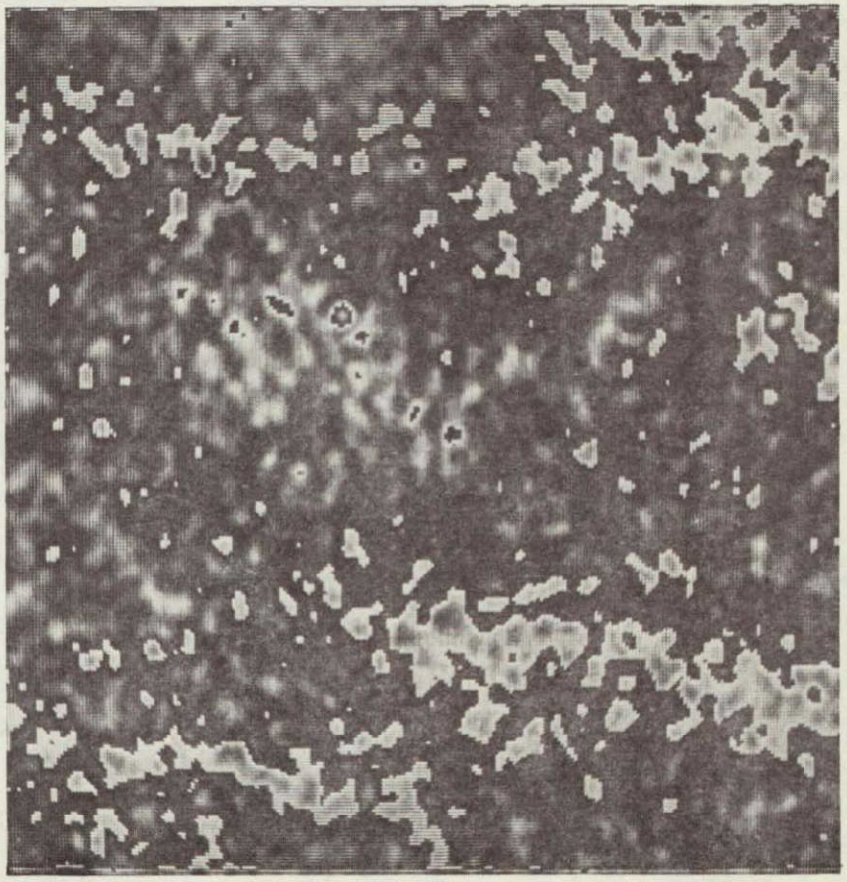

B. Y-3 Contour Map (4°C Interval) (Night)

FIGURE 5.4-1 X-5 and Y-3 Contour Map Comparison of Geysers Area

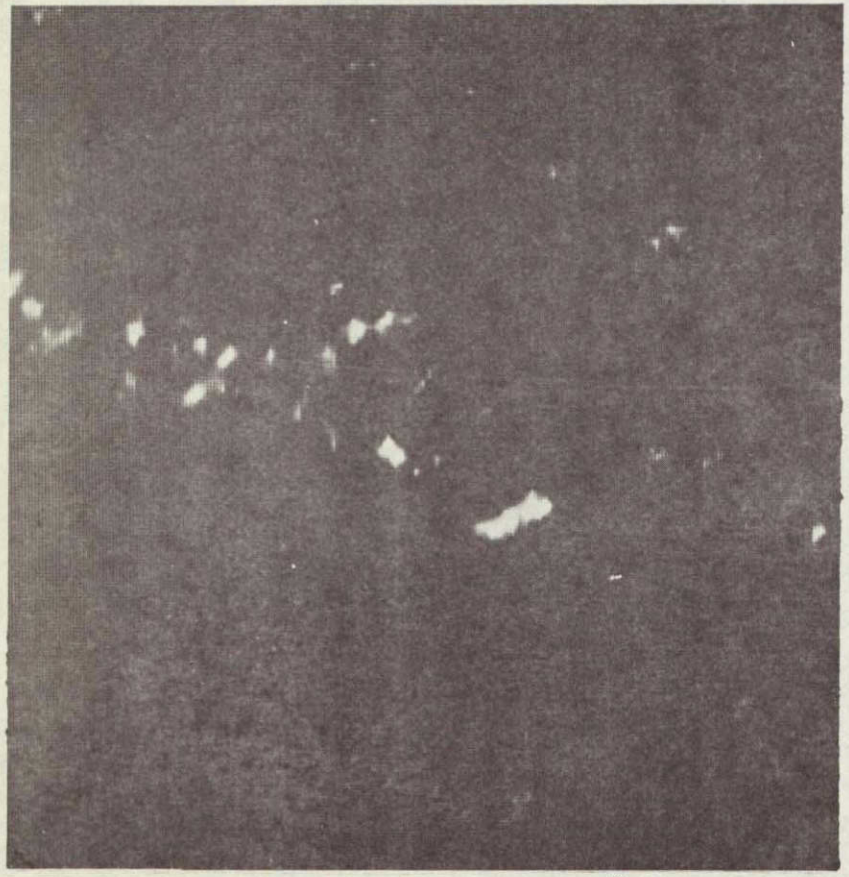

A. Day Hot Spots Above 15°C

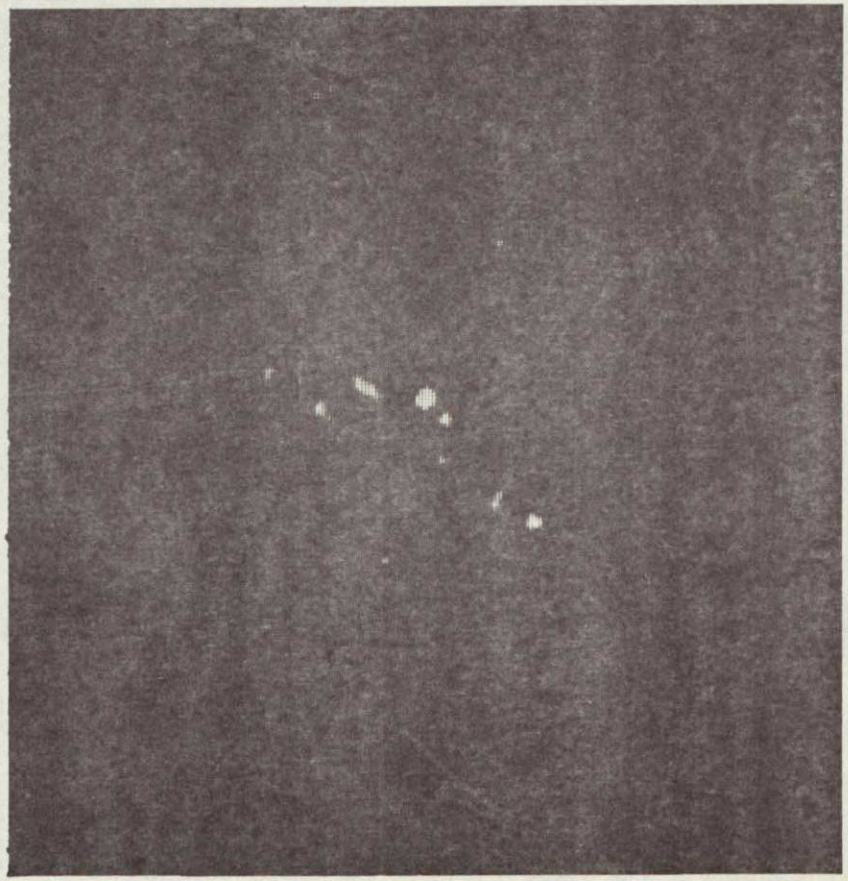

B. Night Hot Spots Above 8°C

FIGURE 5.4-2 Comparison of Day and Night Hot Spots

A. Day X-5

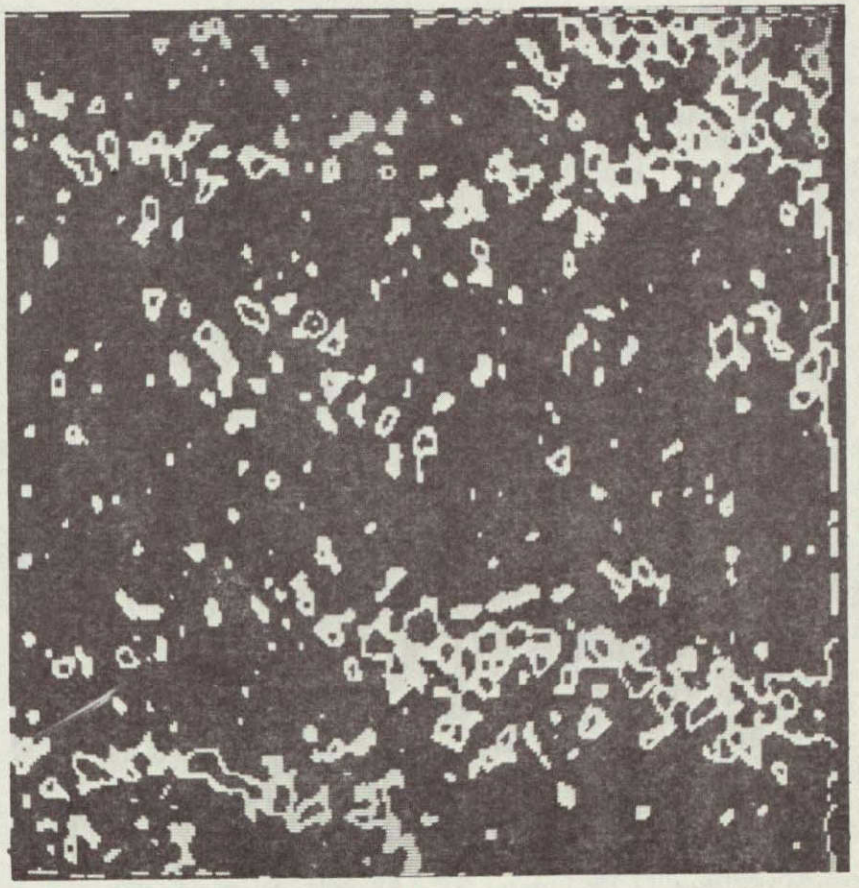

B. Night Y-3

FIGURE 5.4-3 4°C Interval Outline Contours

MSC-05538

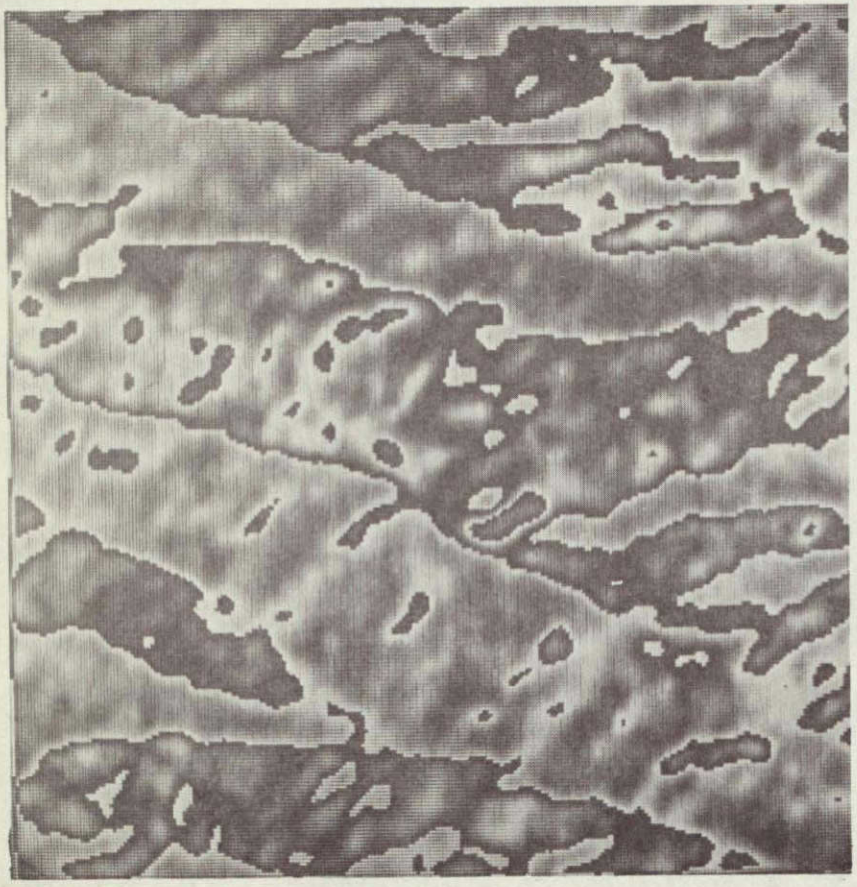

A. Day X-5

B. Night Y-3

FIGURE 5.4-4 8°C Interval Stairstep Contours

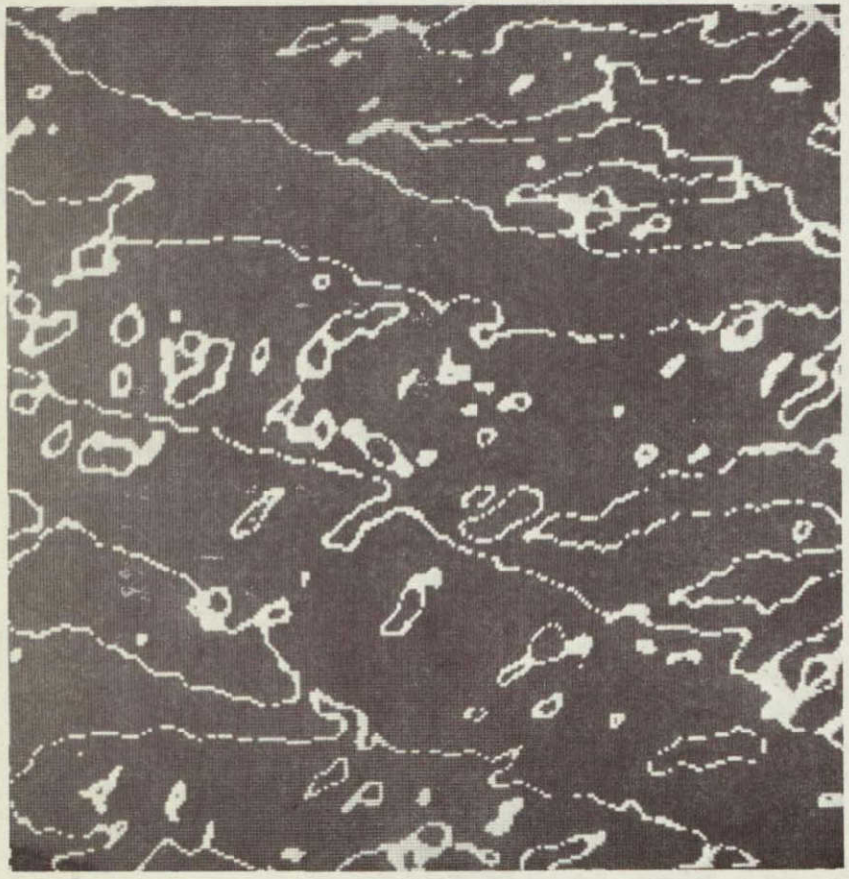

A. Day X-5

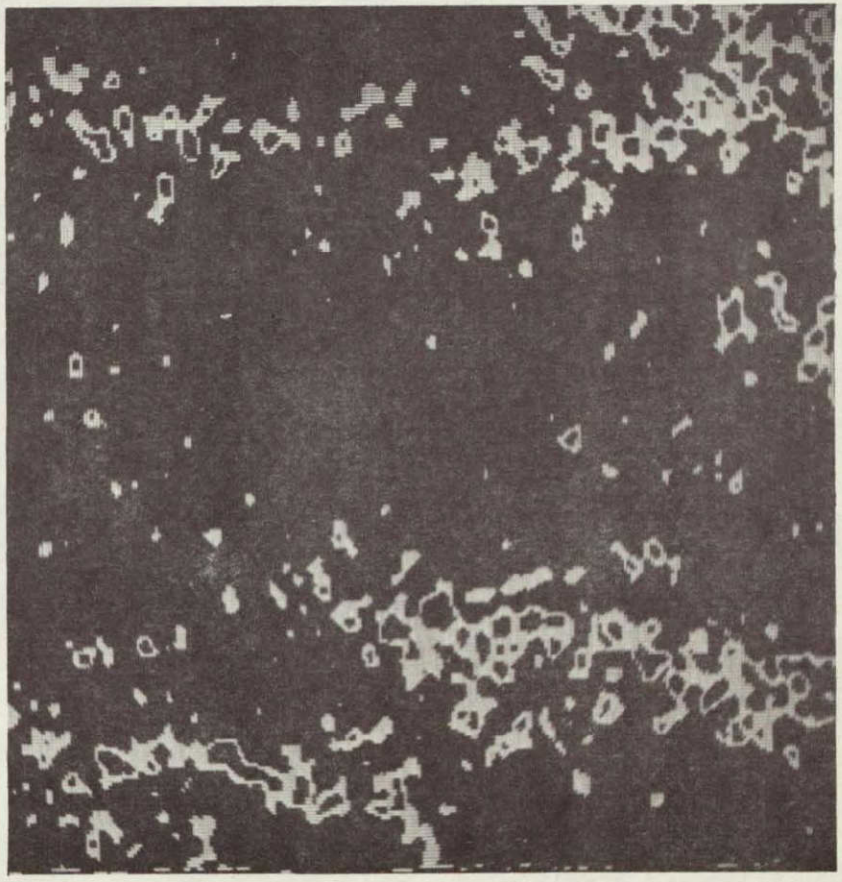

B. Night Y-3

FIGURE 5.4-5 $8^{o}C$ Interval Outline Contours

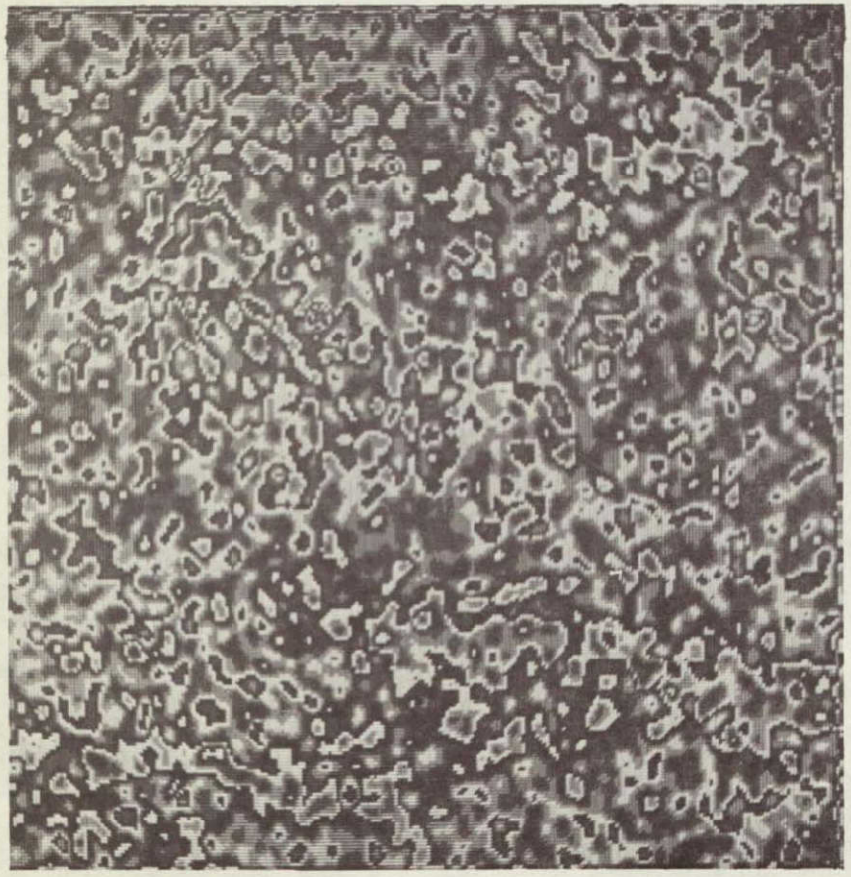

A. Stairstep

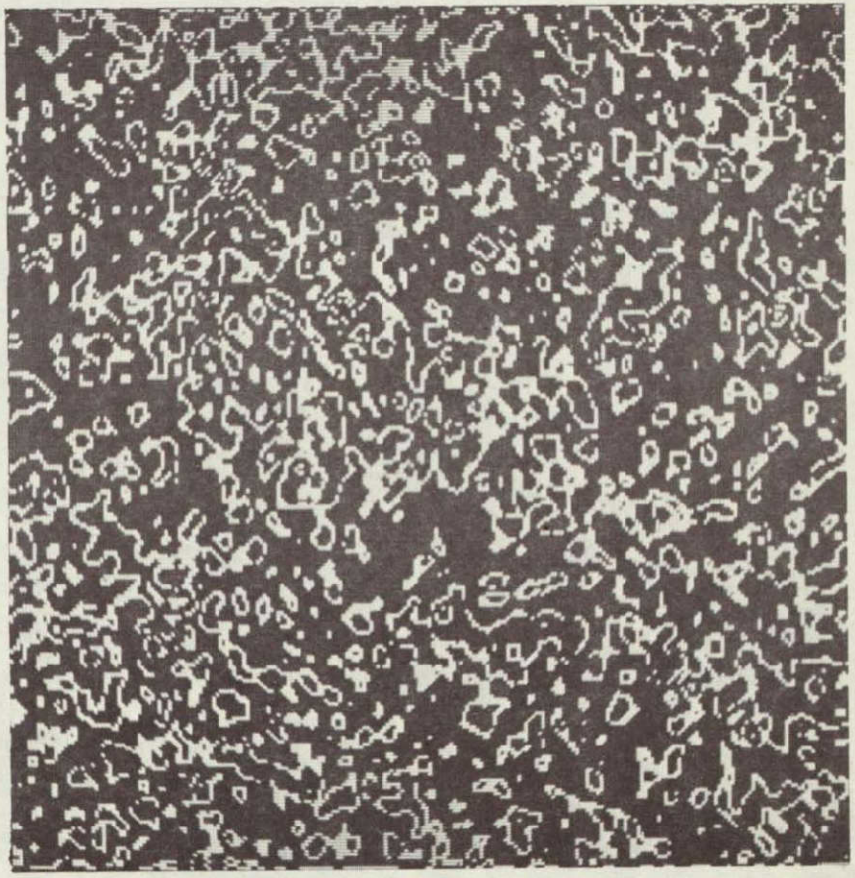

B. Outline

FIGURE 5.4-6 $2^{o}C$ Interval Y-3 Night Contours

6. COMPARISON OF GROUND TRUTH AND S192 DATA

6.1 Atmospheric Temperature Correction - The ground truth data for the December 18, 1973 and January 26, 1974 missions were used to compute the thermal band (10.2 - 12.5 μm) radiance at the S192 entrance aperture. A "compressed line" atmospheric transmission computer program was used which was developed by R. F. Calfee, NOAA, Boulder, Colorado. This program was modified to include the upwelling radiance from each atmospheric layer.

The effect of the atmosphere can be expressed as the difference between the ground based temperature measurement of a ground site and the satellite (S192) based temperature measurement.

For the December mission the computed temperature difference was 0.1^{o}K (ground based temperature minus the S192 based temperature).

For the January mission. this difference was 1.1^{o}K.

6.2 Comparison of Ground Truth Temperature Data with S192 Scanner Data - There are four sets of thermal data over The Geysers area available for comparison. These are:

(1) December 18, 1973 nighttime S192 scanner data (Y-3 detector).

(2) PRT-5 ground truth data taken during the December 18 Skylab overpass.

(3) January 26 daytime S192 scanner data (X-5 detector).

(4) PRT-5 ground truth data taken during the January 26 Skylab overpass.

Figure 6.2-1 shows the typical situation in comparing the January daytime S192 data to PRT-5 radiometer data along a flightline. Except for possible flight path errors and situations where the ground temperature was obviously varying too rapidly, there is plausible agreement. The calculated atmospheric temperature correction of Section 6.1 has been included.

For exact agreement, samples must have come from the same points and the integrating spot sizes been comparable. As discussed in Section 3.5, there was room for error in pointing the PRT-5 radiometer sensor head, locating the helicopter relative to the topographic map and placing the estimated locations of PRT-5 data points on the S192 image for comparison.

The PRT spot size was 60 feet (21.3 meters) in diameter. The instantaneous field of view for S192 was a square 260 feet (79 meters) on a side, and the smoothing algorithm increases this to approximately 650 feet (198 meters).

The comparison (including the atmospheric temperature correction) of the S192 scanner data to the PRT-5 radiometer for the South-North flightline of the December nighttime mission is shown in Figure 6.2-2. There is the probability of possible flight path errors since the location of the helicopter relative to the ground was difficult to determine because of darkness. The EAST-WEST flightline (not shown) was obviously off the intended location although the SOUTH-NORTH flightline (Figure 6.2-2) shows good correlation. The discrepancy of 1.5^{o}C could not be explained by the calculated atmospheric water vapor absorption. A possible cause for this difference is low frequency S192 noise which was not completely removed by processing, as shown in Figure 5.3-2B.

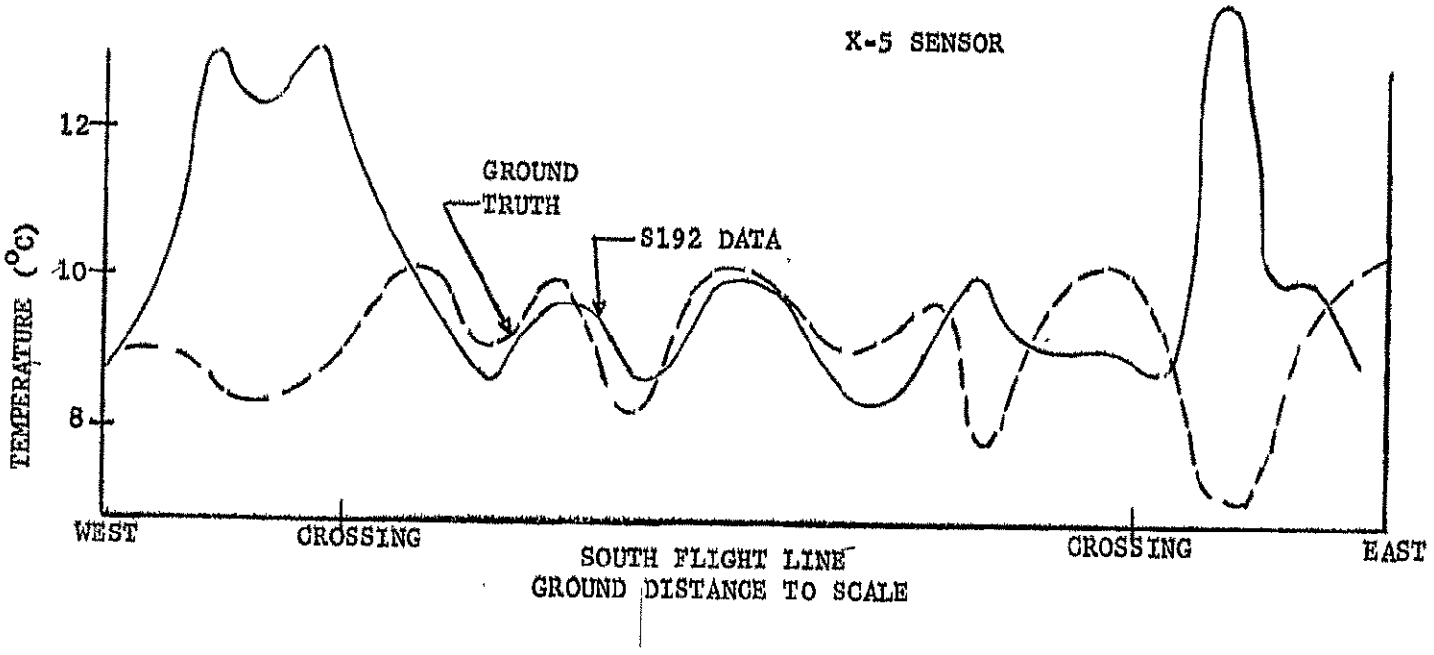

Figure 6.2-1 Comparison of January 26, 1974 (Daytime) Southern East-West Flightline PRT-5 Data (Dashed Line) and S192 Data (Solid line). See Figure 3.7-4 for Location of Flightline.

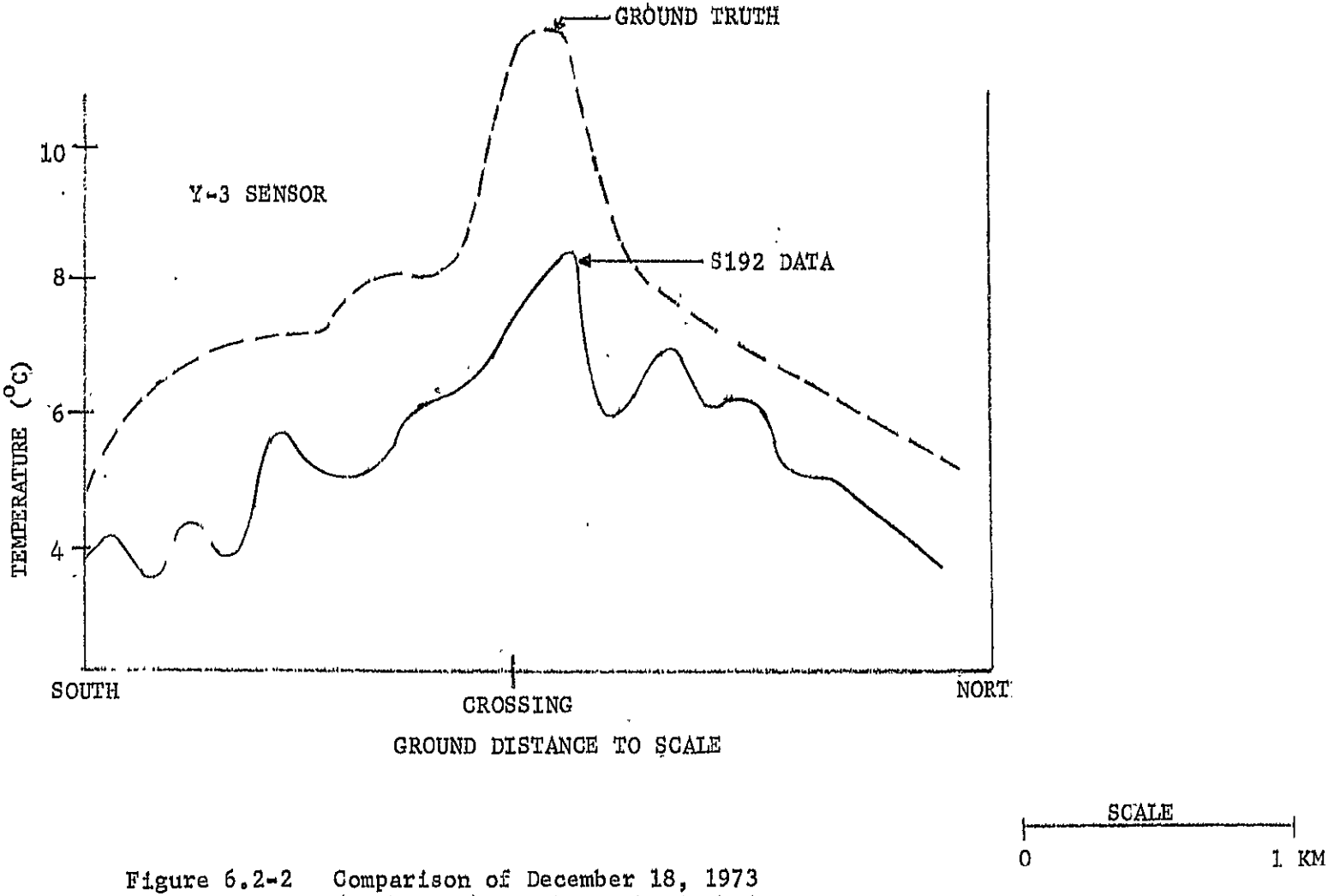

Figure 6.2-2 Comparison of December 18, 1973 (Nighttime) North South Flightline PRT-5 Data (Dashed Line) and S192 Data (Solid Line). See Figure 3.6-4 for Location of Flightline.

7. COMPARISON OF NIGHTTIME (Y-3) AND DAYTIME (X-5) THERMAL BAND IMAGES

There are distinct difference between the thermal band image acquired during predawn hours and the one acquired during daytime. The range of temperatures for the nighttime image is about $10^{o}C$ and about $20^{o}C$ for the daytime image. This difference is due primarily to solar heating with the image structure strongly influence by terrain slope/sun angle relationships. Since the temperature difference attributable to thermal anomalies are independent of the time of day, they are more difficult to distinguish in the daytime image than in the nighttime image.

The nighttime image of The Geysers is shown in Figure 7-1A and the daytime image in Figure 7-1B. Both of these thermal images are stairstep contours with a 4^{o} temperature interval.

A detailed comparison of Figure 7-1 and Figure 3.2-1, which shows the locations of the steam wells and powerplants, resulted in the identification of three powerplant units. The powerplant units #7 and #8 in Figure 3.2-1 are located at "A" in Figure 7-1A and 7-1B. Powerplant unit #11 is located at "B". The hot area located at "S" in the daytime image has no corresponding area in nighttime image and apparently is the result of solar heating.

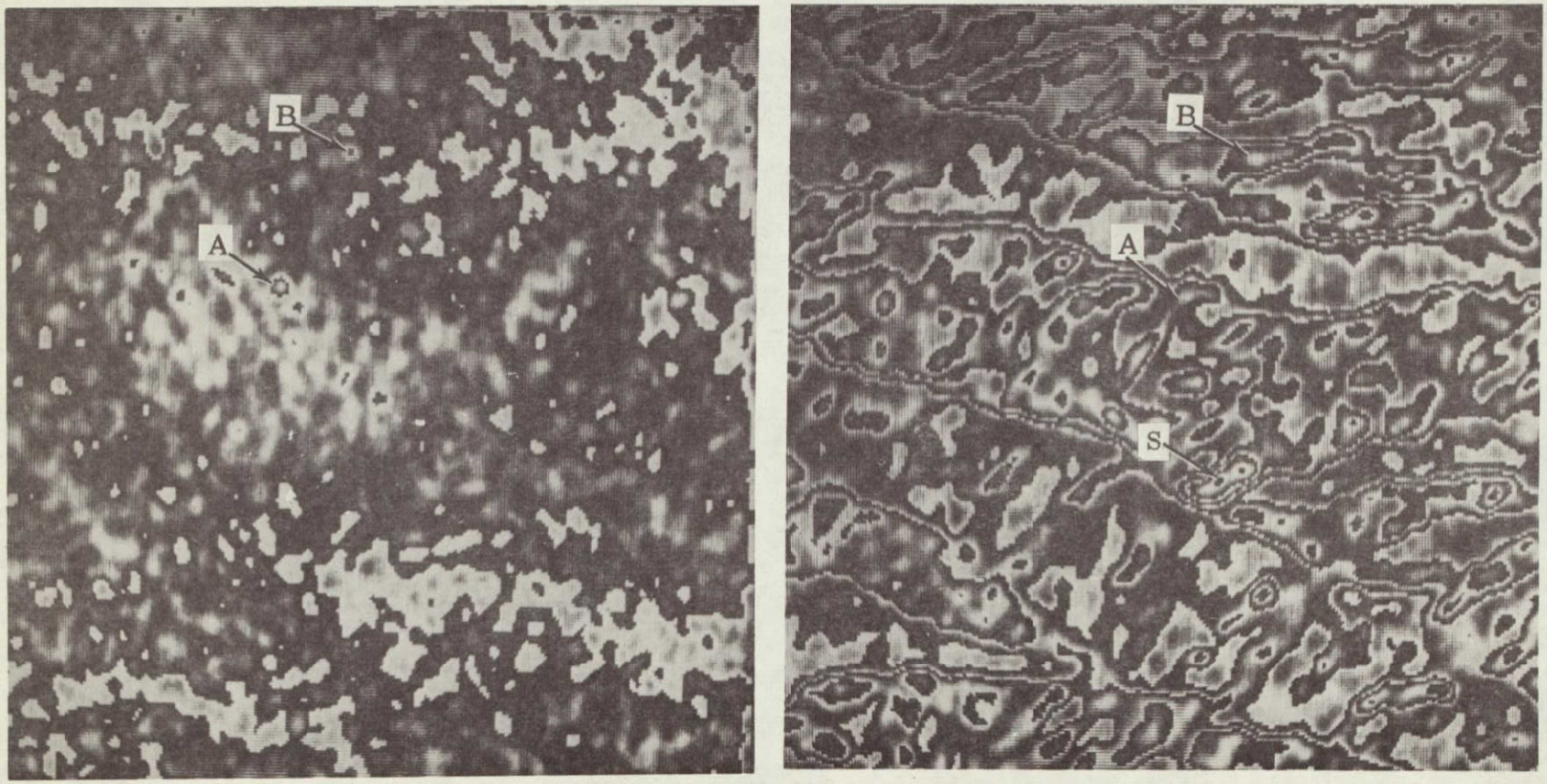

(A) Nighttime - December 18, 1974
Y-3 Sensor

(B) Daytime - January 26, 1974
X-5 Sensor

Figure 7-1 Comparison of Daytime and Nighttime $4^{o}C$ Interval Contour Maps of The Geysers

8. CONCLUSIONS AND RECOMMENDATIONS

Nighttime acquired data are potentially useful in locating geothermal anomalies. With the limited amount of data available for this study, it was not possible to decide conclusively whether or not the geothermal anomalies of The Geysers area would have been detectable without the associated effects of the powerplant development (i.e., cooling towers, steam clouds, barren slopes).

The daytime thermal image is dominated by the effects of solar heating such that no geothermal anomalies could be identified. Daytime images are, however, useful as an interpretation aid for nighttime images of the area to differentiate thermal anomalies due to residual solar heating effects from those that are geothermal manifestations.

In order to fully explore the potential usefulness of S192 data to geothermal exploration, a further study of nighttime thermal images over known, but undeveloped geothermal areas would be required. Daytime images over the same area would also be helpful as an interpretation aid. Surveys of S192 coverage indicate that day-night coverage available for two sites, an extended area in central Mexico north of Mexico City (parallel track coverage) and an area in Nevada (cross-track coverage). However, the possibility of geothermal manifestations in these areas is unknown.

From experience gained in this investigation with S192 thermal contour images, a temperature difference of $0.5^{\circ}C$ is measurable between the background and a square 2 pixels on a side for the X-5 detector array and a square 5 pixels on a side for the Y-3 detector array (1 pixel = 79 meters).

9. NOTES

9.1 References

Allen, E. T. and Day, A. L., 1927, Steam Wells and Other Thermal Activity at "The Geysers" California: Carnegie Inst. Washington pub. 378, 106p.

Bailey, A. W., 1946, Quicksilver deposits of the Western Mayacamas District, Sonoma County, California: California tour. Mines and Geology, v. 42, No. 3, p. 199-230.

Calfee, R. F. and Schweisow, R., New Averaged Infrared Absorption Coefficients of Water Vapor: NOAA Technical Report #ERL 274-WPL24, Boulder, Colorado

Earth Resources Data Format Control Book, PHO-TR543, March 1973*

Earth Resources Production Processing Requirements for EREP Electronic Sensors, PHO-TR524, May 10, 1973*

Garrison, L. E., 1972, Geothermal Steam in The Geysers-Clear Lake Region, California: Geol. Soc. America Bull, V. 83, p. 1449-1468.

McNitt, J. R., 1963 (Revised 1965), Exploration and Development of Geothermal Power in California: California Div. Mines and Geology, Spec. Rept. 75, 45p.

McNitt, J. R., 1968, Geology of the Kelseyville Quadrangle, California: California Div. Mines and Geology, Map Sheet 9.

Moxham, R. M., 1969, Aerial Infrared Surveys at the Geysers Geothermal Steam Field, California: U.S. Geo. Survey Professional Paper 650-C, p. 106-122.

* This document is periodically updated; this data reflects the last known publication or change.

APPENDIX A

Image Processing Facility and Software

A.1 INTRODUCTION

Martin Marietta Corporation, Denver Division, is engaged in an internal research program in the area of image processing. The experience directly relates to the problems of feature correlation, digitalization, and volume screening; and to determination of feasible system processes for exploiting digitally encoded image data. This experience has sufficient breadth and depth for adapting to the many image processing requirements. One evidence of this is the fact that an experimental digital image processing facility has been set up and the problems of software, hardware and algorithmic techniques have been successfully tackled. A second evidence is the fact that the internal research and development program in image processing has been continuously supported since 1969 with sufficient resources to handle the wide spectrum of necessary disciplines and technologies Activities include internal research and development programs (IRAD), contracts, and new business and spans the areas of data management, computer software techniques, computer hardware and integration techniques, optical processing, radar and electronic intelligence systems, and imagery analysis.

A.2 IMAGE PROCESSING FACILITY

As a consequence of these image processing tasks and associated facility expenditures, a working experimental image processing facility has been developed where candidate image processing methods can be analyzed, simulated, and designed and where results can be quickly evaluated in regard to user requirements. Both hardware and software aspects were considered in the engineering and the system uses an interactive conversational mode of programming. The system has the features of a large disc unit (2.5 million words, 16 bits/word), an image digitalization and display unit, two IBM/CDC compatible tape storage units, a general purpose 65000 word (16 bit/word) computer (SEL-72 using virtual memory), and a special purpose 8000 word computer. Fortran, Basic, and assembly languages as well as editing, loading and debugging are part of its basic SEL-72 software. An extensive library of image and processing software has been generated including a command monitor language to control this processing software. The processing monitor operations can be controlled from Fortran thus providing the user with a high level language access to the specialized processor software. There are also provisions for subroutine, data, and disk linkages between the various software systems. A card reader and a line printer are interfaced to provide a more flexible input-output capability. The system has a high speed graphic oscilloscope terminal and a teletype terminal as the control peripherals.

The digitalization is done under software control for any of the following: (1) determination of scan pattern, (2) display images on a high quality precision oscilloscope, (3) fetching images from a high quality image dissector camera, and (4) changing the sampling frequency. A precision light table was interfaced to provide two axis alignment and film advance. A wide variety of film sizes, film formats and scan data formats can be accommodated.

A.3 IMAGE PROCESSING OPERATIONS

An image monitor software package has been developed with 71 operational commands. It is used to do image operations such as correlation studies, feature extraction, image screening, two dimensional Fourier transforms, convolution studies, and digital filtering studies. Figure A-1 shows the structure of the image processing system employed. This structure was found to be essential in order to achieve the results of this report. The large amount of programming work necessary to establish a workable image processing capability has been accomplished including:

1) Monitor subprocedure and conditional sequence control commands.

2) Image sub-blocking and scan conversion routines.

3) Random access core to disc data management commands.

4) Scanning, digitalization and display of images.

5) Dynamic core area allocation and buffer sizing to allow effective use of the core size.

6) An extensive library of histogram, graphing, statistical and data study routines.

7) A compatible tape writing and reading routine for IBM and CDC formats.

8) Parameter table assignment system to allow dynamic exchange of constants and operation data during processing.

9) Several point intensity commands such as scaling, biasing, thresholding, logarithmic contrast expansion and compression, and non-linear operations.

(10) A fast two-dimensional Fourier transform using fixed point arithmetic and batch scaling, including centering, bit reversal, and radial filtering routines. This is important because of the relation of correlation operators to transforms.

(11) Convolution, correlation, and digital filtering routines which relate to many effective and efficient processing techniques such as feature extraction, noise elimination, template screening, enhancement, and image separation.

(12) The Walsh-Hadamard transform routine for research in new algorithmic techniques.

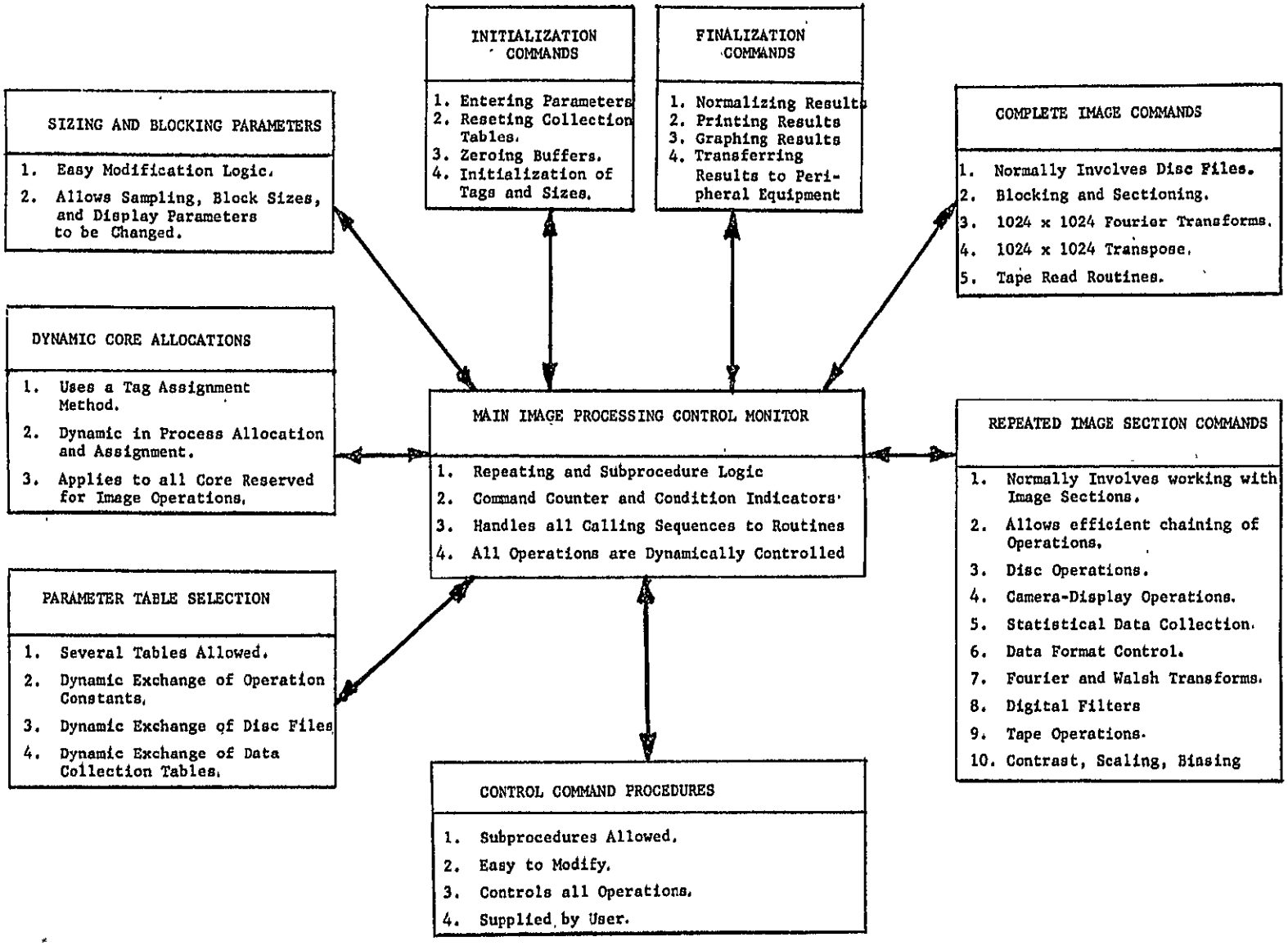

FIGURE A-1

SEL-72 MINICOMPUTER IMAGE PROCESSING SOFTWARE SYSTEM

APPENDIX B

Differential Offset Algorithm Details

B. DIFFERENTIAL OFFSET ALGORITHM DETAILS

Software for tape reading, contouring, enlargement area selection, geometric correction and filtering was developed. The software is in assembler code for the System Engineering Laboratories Model SEL-72 computer and contains details not relevant to most readers of this report. However, the algorithm for calibrated dynamic offset revision is a principal result of this report, therefore, complete details are provided, suitable for direct coding of the algorithm on almost any computer system, whether done in assembler or a higher level language. Our implementation used a random access disc peripheral.

Two types of variables are exhibited in various flowcharts and diagrams. The first is a core pointer variable which may be either absolute or relative. The second is a data variable which may be located in core by a pointer variable. In higher level language, such as FORTRAN, the pointers would be array indexes and the relative mode of reference would be chosen internal to a routine.

It is possible to design more efficient algorithms which employ two dimensional moving averages. In our implementation, some computation is done over for each line, and one dimensional techniques are used. The one dimensional moving average concept is to modify the average by adding a new point to the right and dropping a point to the left.

The calibrated dynamic offset is achieved by a difference of moving averages. High and Low calibration values are the first two items of a scan line, and these are averaged before the final equation is applied.

Table B-1 provides a dictionary of variables for the algorithm. Figure B-1 provides the geometry used. Only 33 scan lines of data are in core at once. The pointers are advanced each time a new line is brought in. Old data is not moved. Figures B-2 to B-5 are flow charts which show everything but disc operations. The disc operations routines are READ and WRITE. These routines allow the record to be sized, and random accessed and transferred to or from a specified buffer.

TABLE B-1

LIST OF VARIABLES
FOR CALIBRATION AND DYNAMIC
OFFSET REVISION ROUTINE

CALBDYRV	Driver Section for Disc to Disc File Output
BASEIN	Pointer to First Location of Input Array (A)
BASEOUT	Pointer to First Location of Output Array (A)
MDK	Length of Scan Line Being Processed
MX	Length of Segment of Scan Line
MY	Number of Scan Lines in Input Array
INRECNT	Input Random Access Disc Record Pointer
OURECNT	Output Random Access Disc Record Pointer
FRSTLINE	Pointer to the Lowest Scan Line in Input Array (A)
LASTLINE	Pointer to Last Location +1 of Input Array (A)
ROWPNT	Pointer to Scan Line Containing Segment (R)
ROWSTOP	Limit for ROWPNT (R)
OUTSTOP	Limit for OURECNT (R)
SLABAVGR	Slab Average Computation Section
ROBSPNT	Pointer to Scan Line Containing Segment (A)
SQSUM	Accumulator of Sum of Pixels in Square
ROWSUM	Accumulator of Sum of Pixels in Segment
HCALAVG	High Calibration Average Value
LCALAVG	Low Calibration Average Value
USEBSE	Dummy Pointer (A)
USECNT	Dummy Counter (R)
STOPBSE	Dummy Limit (A)
CALUSE	Pointer to Pixel to be Calibrated (R)
CALSTOP	Limit for Pixels to be Calibrated (R)
OLDPNT	Lookback Pointer to Pixel to be Dropped Off (R)
NEWPNT	Lookahead Pointer to Pixel to be Added On (R)
CALIBRAT	Actual Calibration Computation Section
ROWAVG	Average of Pixels in Segment
SQAVG	Average of Pixels in Square
JUMPSUM	Performs Sampled Addition
READ	Fetches a Scan Line Record from Disc
WRITE	Writes a Scan Line Record to a Second Disc

Absolute Pointers Point to Actual Locations in Core (A)
Relative Pointers are Relative to Some Origin and Begin at Zero (R)
Limits Point to Last Element + 1 (Based or Unbased)

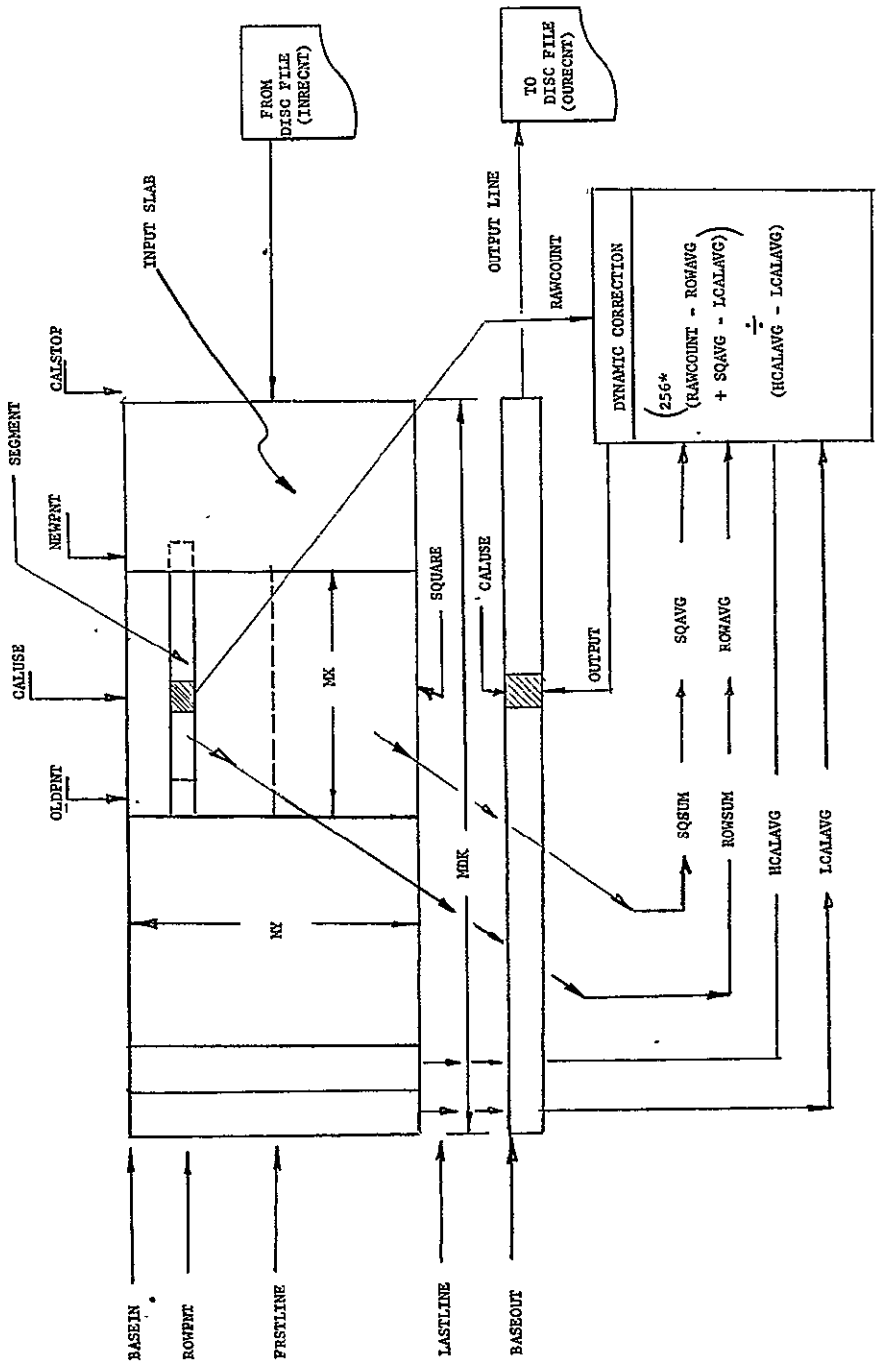

FIGURE B-1 Dynamic Offset Geometry

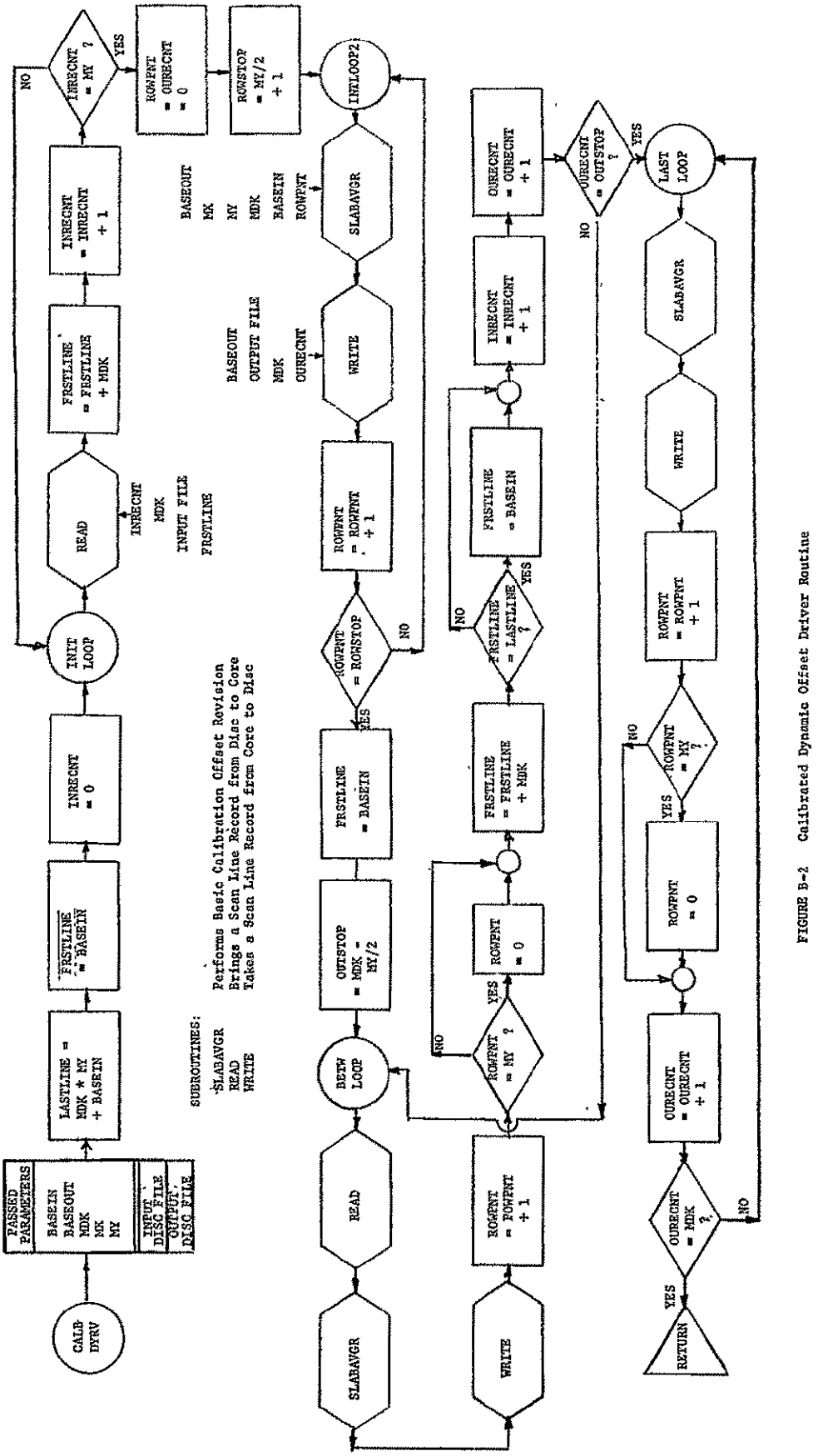

FIGURE B-2 Calibrated Dynamic Offset Driver Routine

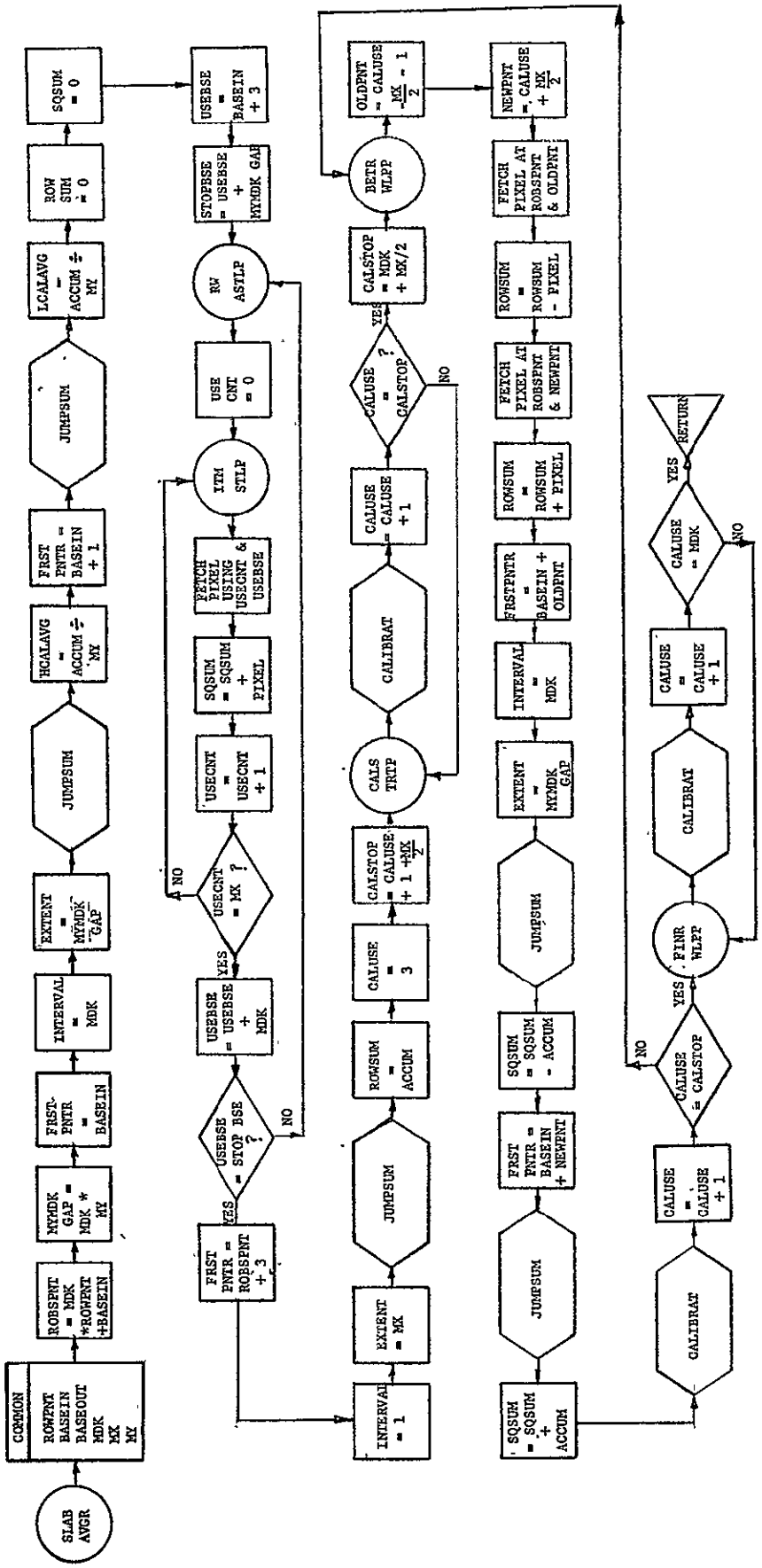

FIGURE B-3 Scan Line Operating Routine

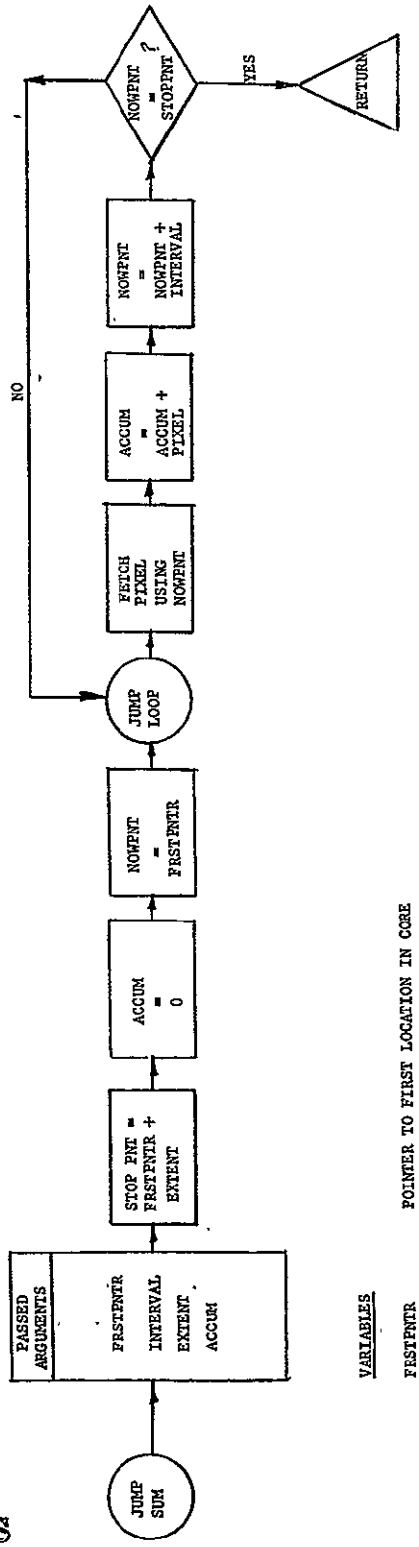

VARIABLES

FRSTPNTR	POINTER TO FIRST LOCATION IN CORE
INTERVAL	SPACING BETWEEN PIXELS IN CORE
EXTENT	NUMBER OF POINTS TIMES INTERVAL
ACCUM	FINAL RESULT ACCUMULATOR

FIGURE B-4 Sampled Accumulation Routine

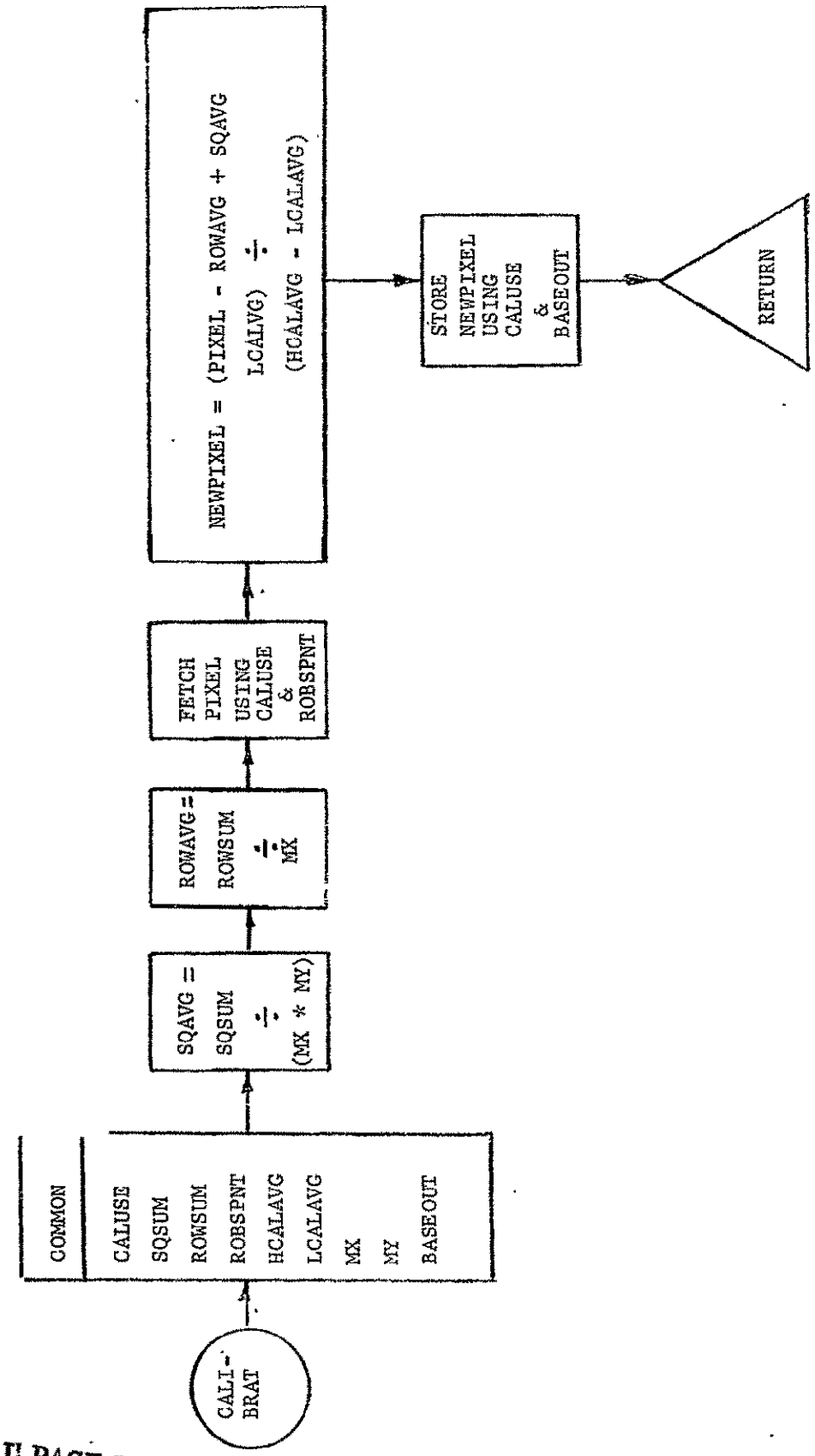

FIGURE B-5 Calibration and Offset Computation